ULTRASOUND AND NUCLEAR MAGNETISM IN BULK AND CONFINED LIQUID HELIUM-3

By

BRADLEY NEAL ENGEL

A DISSERTATION PRESENTED TO THE GRADUATE SCHOOL
OF THE UNIVERSITY OF FLORIDA IN PARTIAL FULFILLMENT
OF THE REQUIREMENTS FOR THE DEGREE OF
DOCTOR OF PHILOSOPHY

UNIVERSITY OF FLORIDA

1988

UNIVERSITY OF FLORIDA LIBRARIES

ACKNOWLEDGEMENTS

First, I would like to thank my research advisor and good friend, Professor Gary Ihas, for his guidance and unshakable support during the 31 % of my life that I have known him. He gave me my first opportunity in experimental research when I was just a naïve undergraduate who thought that all physics experiments could be purchased from the "Edmund Scientific" catalog. Over the years, Gary has been a endless source of ideas and knowledge and yet has given me the freedom necessary to become an independent researcher. Finally, he has always been there as a friend to help me through the numerous low points.

I would also like to thank the two other graduates from this lab, Dr. Bobby Berg and Dr. Greg "Speedo" Spencer. Their acceptance of me as an equal from my very first days in the lab allowed me to understand physics research first hand at an early age. I especially feel a debt of gratitude for having had access to their operating experiments. The data for this dissertation are a result of being able to use their well built cells for other purposes. I hope that I leave such useful apparatus for future students.

Many thanks go to my friends and colleagues here at Florida. Professors Dwight Adams and Neil Sullivan have always been encouraging and helpful. Dr. Steve Herr showed me that it was not that bad to be single. My fellow graduate student, Major Jack Killian, has always been a source of boundless optimism. Thanks are extended to Larry Frederick for his enthusiastic production of electronics needed for the experiments.

And finally I offer a thank you to my family. I would like to give special credit to my brother Matt, for his revealing to me the wonders of building things.

It was his inclusion of me in all of his projects and hobbies that truly trained me to be an experimentalist. And of course, my mother Beatrice was always there. It would only take a phone call to hear her say "Of course you'll finish" to get me back on track. And last, I would like to thank my friend for life, Kristine Griffin. She was always supportive through the trying times my life in the lab put us through.

TABLE OF CONTENTS

		page
ACKNOWLEDGEMENTS		ii
LIST OF FIGURES		vi
ABSTRACT		viii
CHAPTERS		
1	INTRODUCTION	1
2	THEORETICAL AND EXPERIMENTAL REVIEW	5
	Introduction	5
	Normal Liquid ^{3}He and Landau's Fermi Liquid Theory	5
	Sound in Superfluid ^{3}He	13
	Surface Magnetism of ^{3}He	16
	Experimental Review	16
	Theoretical Review	28
3	EXPERIMENTAL APPARATUS AND TECHNIQUE	33
	Refrigeration	33
	Experimental Cell Heat Exchanger	34
	Thermometry	35
	Ultrasound Techniques	37
	NMR techniques	41
	Experimental Cells	46
	Data Aquisition	52
4	ULTRASOUND RESULTS IN LIQUID ^{3}He	53
	Introduction	53
	Identification of Attenuation Satellites	53
	Velocity Measurements at T=0	58
	Pressure Dependence of F_0^s	63
	Conclusions	69
5	NMR MEASUREMENTS OF ^{3}He IN VYCOR	71
	Introduction	71
	NMR Measurements	71
	Magnetic Susceptibility	75

Spin Lattice Relaxation 85
Measured Spin Dephasing Time, T_2^* 90
Deduction of Spin–Spin relaxation time, T_2 90
Magnetism and Flow Interactions 97
Conclusions 103

6 CONCLUSIONS AND FUTURE WORK 104

REFERENCES 107

BIOGRAPHICAL SKETCH 110

LIST OF FIGURES

1–1	Low temperature ^{3}He phase diagram	3
2–1	Zero–sound velocity and attenuation	14
2–2	Ultrasound velocity and attenuation in superfluid ^{3}He	17
2–3	Susceptibility vs coverage of ^{3}He on Vycor	19
2–4	$\chi T/C$ vs T for ^{3}He filled Vycor	21
2–4	γ_3^* vs T for ^{3}He in carbon particles	23
2–6	Frequency shift of ^{3}He in Grafoil	25
2–7	Magnetization vs coverage for ^{3}He on Grafoil	29
2–8	Models for ^{3}He surface magnetism	30
3–1	Ultrasound electronics	38
3–2	Pulsed NMR electronics	42
3–3	CW NMR electronics	45
3–4	Ultrasound apparatus	47
3–5	Pressure control loop	48
3–6	Vycor cell	50
3–7	Detail of Vycor rod	51
4–1	Raw sound amplitude below T_c	55
4–2	Phasor diagram of sound interference	57
4–3	Sound amplitude corrected for interference	59
4–4	Superfluid zero–sound velocity and attenuation vs pressure	60
4–5	T=0 asymptotic velocity	62
4–6	$(c_0-c_1)/c_1$ vs pressure	65

4–7	$F_{\frac{1}{2}}$ vs pressure	66
4–8	$F_{\frac{1}{2}}$ as compared with older work	67
4–9	Comparisons to $F_{\frac{1}{2}}$ derived from transverse sound	69
5–1	Digitized FID	73
5–2	Digitized CW line	74
5–3	Heat pulse recovery	76
5–4a	χ^{-1} vs T at 0 bars	77
5–4b	χ^{-1} vs T at 2 bars	78
5–4c	χ^{-1} vs T at 3 bars	79
5–4d	χ^{-1} vs T at 5 bars	80
5–4e	χ^{-1} vs T at 7 bars	81
5–4f	χ^{-1} vs T at 9 bars	82
5–5	Curie–Weiss fit to χ^{-1} vs T	84
5–6	χ^{-1} vs T to high T	86
5–7	Weiss δ vs pressure	87
5–8	τ_1 vs temperature	88
5–9	τ_1 of Si spins in Vycor	89
5–10	τ_2^* vs T for five frequencies	92
5–11	τ_2^{*-1} vs frequency	93
5–12	$\Delta H/H$ vs T	94
5–13	Deduced τ_2 vs T	96
5–14	τ_2^* vs T with curves from model	98
5–15	χ response to flow	99
5–16	Fit to τ_2^* vs T	101
5–17	Flow on χ with heating effect removed	102

Abstract of Dissertation Presented to the Graduate School
of the University of Florida in Partial Fulfillment of the
Requirements for the Degree of Doctor of Philosophy

ULTRASOUND AND NUCLEAR MAGNETISM IN BULK AND CONFINED LIQUID HELIUM–3

By

Bradley Neal Engel

August 1988

Chairman: Professor Gary G. Ihas
Major Department: Department of Physics

Two different experiments on liquid ^{3}He in open and confined geometries were performed. In the first, the attenuation and velocity of 5 MHz ultra–sound were measured in both the bulk normal and superfluid phases as a function of temperature (0.3 to 30 mK) and pressure (0.3 to 34 bars). The zero temperature limiting behavior was observed in the B–phase superfluid at temperatures below $T/T_c=0.4$. The velocity was found to return to its ordinary first–sound value as was theoretically expected. Using precise measurements of the difference between the zero– and first–sound velocities, the second symmetric Landau parameter, F_2^s, was deduced as a function of pressure.

In the other experiment, nuclear magnetic resonance (NMR) was used to probe the magnetic susceptibility, χ, transverse spin dephasing time, T_2^*, and spin–lattice relaxation time, T_1. Measurements were performed as a function of temperature (0.3 mK to 2 K), pressure (0 to 9 bars), and frequency (231, 345, 462, 692, and 924 kHz). The magnetic susceptibility was found to obey a Curie–Weiss

law with a pressure–dependent ferromagnetic Weiss temperature. The spin dephasing time was found to be a strong function of temperature at low temperature, with its slope determined by the resonance frequency. This frequency dependence of τ_2^* was exploited, using a simple model, to obtain the true spin–spin relaxation time, τ_2, as a function of temperature. This was found to obey the same inverse temperature dependence as the susceptibility, diverging at the extrapolated ferromagnetic transition.

CHAPTER 1
INTRODUCTION

The most often asked question by the uninitiated upon entering an ultra-low temperature laboratory is "Why do you want to get things so cold?" Many versions of the answer exist. Some are very grandiose soliloquies on the fundamental interactions of nature, while others delve into the very specialized details of a particular problem. But, the pure essence of physics research can be embodied by one simple answer, "To see what happens." As the last eighty years since the liquefaction of helium by Kammerlingh-Onnes have shown, quite a lot of things do happen near absolute zero.

The term "low temperature" is a relative one. In the study of a particular physical problem, the relevant temperature scale is set by the interaction energies of the system. To be at "low temperature" then, requires only that the energy of a thermal excitation (on the order of $k_B T$, where k_B is Boltzmann's constant) be small enough so as to not disturb the interactions of interest. A good example of this is the behavior of the free electrons in a metal at room temperature. The electrons are well described by the theory of a free Fermi gas near its ground state. Hence, they are displaying their low temperature limiting behavior at room temperature because the relevant energy, the Fermi energy, is equivalent to several thousand degrees.

Many interesting systems in physics have inter-particle forces which are very weak and, therefore, are totally masked by the constant thermal excitations present at ordinary temperatures. For a true understanding of the physical processes governing a system, its behavior in the absence of this thermal agitation must be

studied. This is the motivation for attaining low temperatures. Once a theoretical model based on the behavior at absolute zero is formed, the effect of thermal excitations can be added in a controlled way. A complete picture will contain enough information to predict the behavior from T=0 up to finite temperatures. Low temperature studies provide the experimental realization of the "ideal" system for the theory to try to explain.

Because, at low temperatures, the low energy interactions are allowed to dominate, long range order can form in the system. For example, the particles in a superfluid become correlated over distances large compared to their inter–particle spacing. In a magnetic system, the magnetic moments can align with each other to form an ordered state throughout the sample. The two experiments performed for this dissertation explore the tendency toward order in two different systems based on the light isotope of helium, ^{3}He.

The first experiment was an ultrasound study of both the normal Fermi liquid and superfluid states of liquid ^{3}He. Figure 1–1 is a representation of the low temperature phase diagram of ^{3}He displaying the temperature, pressure and magnetic field dependences of the states. The attenuation and phase velocity of 5 MHz ultrasound was measured as a function of temperature (0.3 to 30 mK) and pressure (0.3 to 34 bars). The first result of these measurements (Engel et al., 1985) was the identification of the cause of temperature dependent attenuation satellite peaks in superfluid ^{3}He–B that had previously been reported (Paulson and Wheatley, 1978). The origin of these peaks is an interference between the propagated sound pulse and an excitation of the receiving sound transducer from unwanted electromagnetic leakage. With the origin of this effect understood, additional measurements were made to eliminate it in the analysis. This allowed the true attenuation and velocity to be measured (Ihas et al., 1985).

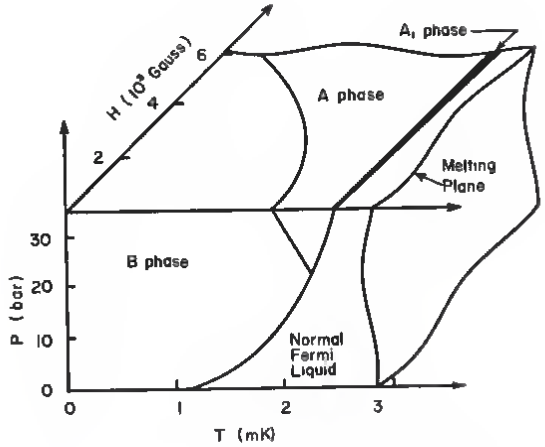

Figure 1–1 Low temperature phase diagram of ^{3}He.

The ability to cool this ultrasound cell to temperatures previously unattained allowed the zero temperature limiting behavior of the sound velocity and attenuation to be observed. The sound velocity in the B–phase superfluid was found (Engel and Ihas, 1985) to approach its theoretically predicted value (Wölfle, 1973). Using the difference between this asymptotic value and that measured at the superfluid transition, T_c, the second symmetric Landau parameter, F_2^s, was deduced as a function of pressure (Engel and Ihas, 1985).

The other experiment performed was a nuclear magnetic resonance (NMR) study of liquid ^{3}He confined in the pores of Vycor glass. This system displays an enhanced magnetic susceptibility over that of the bulk liquid as first reported by Brewer (1970). The magnetic susceptibility, χ, transverse spin dephasing time, τ_2^*, and spin–lattice relaxation time, τ_1, were measured as a function of temperature, pressure, and magnetic field. The susceptibility was found to obey a Curie–Weiss law with a pressure dependent Weiss temperature. A simple model for the magnetic field dependence of τ_2^* is presented and the actual spin–spin relaxation time, τ_2, is deduced. Finally, some interesting flow–magnetism interactions are presented.

CHAPTER 2

THEORETICAL AND EXPERIMENTAL REVIEW

Introduction

This chapter is intended as a short review of the relevant theoretical ideas and experimental results necessary for an understanding of the work presented in this dissertation. The following is divided into three sections: one on normal liquid ^{3}He and Landau's Fermi liquid theory following Leggett (1975) and Wölfle (1978), a brief section on Superfluid ^{3}He with emphasis on sound propagation, and the final one on the enhanced magnetism of ^{3}He in confined geometries.

Normal Liquid ^{3}He and Landau's Fermi Liquid Theory

The properties and responses of liquid ^{3}He at temperatures well below the Fermi temperature of $\approx$1 K ($T \lesssim 100$ mK) but above the superfluid transition can be well accounted for by a model due to Landau (1956 and 1957) called the Fermi liquid. This model begins with a system of non–interacting spin $\frac{1}{2}$ particles and adiabatically turns on the interaction between the particles. If the individual atoms are now imagined to collect a screening cloud of other atoms around them, the problem can be reformulated in terms of these dressed atoms or *quasiparticles* whose interactions can be accounted for more easily.

In a non–interacting gas of N spin $\frac{1}{2}$ particles, the single particle eigenstates are plane–wave states of momentum $\mathbf{p}$, spin projection $\sigma_z = \pm\frac{1}{2}$ and energy

$$\epsilon_p = \frac{p^2}{2m} = \frac{(\hbar k)^2}{2m} \tag{2.1}$$

where $\mathbf{k}$ is the wavevector corresponding to $\mathbf{p}$. If now periodic boundary conditions are imposed, the ground state is the so-called *Fermi sea*: all single-particle states are filled up to a limiting momentum, the Fermi momentum,

$$p_F = \hbar k_F = \hbar(3\pi^2 N)^{\frac{1}{3}} \tag{2.2}$$

Similarly, one defines the Fermi energy and velocity as

$$\epsilon_F \equiv \frac{p_F^2}{2m} \tag{2.3}$$

$$v_F = (d\epsilon/dp)_{p_F} = \frac{p_F}{m} \tag{2.4}$$

At low temperatures, single particles may be excited into states just above the Fermi surface. Thus, the low temperature static properties are determined entirely by the density of states at the Fermi surface

$$N_F = \left[\frac{dn}{d\epsilon}\right] = \frac{3N/n}{2\epsilon_F} \tag{2.5}$$

For example, the magnetic susceptibility and specific heat are given by

$$\chi = \tfrac{1}{4}\gamma^2\hbar^2(dn/d\epsilon), \qquad C_v = (\pi^2/3)k_B^2(dn/d\epsilon)T \tag{2.6}$$

From the free Fermi gas one can obtain the full interacting system. When the inter–particle potential is adiabatically turned on, the particles of mass m are now replaced by *quasiparticles* with some effective mass, m*, reflecting this interaction. Hence, the number of quasiparticles is equal to the number of atoms in the system, N. As before, the quasiparticles occupy plane–wave eigenstates of momentum p and spin projection $\sigma = \pm\frac{1}{2}$ and must obey the Pauli exclusion principle. And, the ground state is the Fermi sphere filled up to the Fermi momentum as given for the free gas in equation (2.2). The quasiparticle distribution function is the same as for fermions

$$n_{p\sigma}(\epsilon) = \left[\exp\left[\frac{\epsilon-\mu}{k_B T}\right] + 1\right]^{-1} \tag{2.7}$$

which at low temperatures differs from a step function only near the chemical potential, μ. Now, the density of states at the Fermi surface is that for the free gas modified by the effective mass, m*

$$N_F = \frac{3Mm^*}{p_F} \tag{2.8}$$

For ^{3}He, m*/m varies from about 3 at low pressure to about 6 at the melting pressure. If this were all that was needed, the properties of the degenerate liquid would be those of the free gas with m replaced by m*. However, the highly interacting system is far richer than that. To account for these strong interactions between the atoms, a parameterization of the interactions between the quasiparticles is introduced.

Because the energy of a quasiparticle depends on the configuration of the surrounding quasiparticles, a local change in the distribution function $\delta n_{p\sigma}(r,t)$

causes the quasiparticle energy to change by an amount

$$\delta\varepsilon_{p\sigma}(\mathbf{r},t) = \sum_{\mathbf{p}'_s\sigma'} f_{p\sigma\,\mathbf{p}'\sigma'}\ \delta n_{\mathbf{p}'\sigma'}(\mathbf{r},t) \tag{2.9}$$

where $f_{p\sigma\ p'\sigma'}$ is the Fermi liquid interaction introduced by Landau This interaction may be rewritten in terms of the angle of scattering between two quasiparticles as

$$f_{p\sigma\ p'\sigma'} = N_f^{-1}\sum_{l=0}^{\infty} P_l(\hat{p}\cdot\hat{p}')(F_l^s\delta_{\sigma\sigma'} + F_l^a\sigma\cdot\sigma') \tag{2.10}$$

where $P_l(\cos\theta)$ are the Legendre polynomials and $\hat{p} = \mathbf{p}/|\mathbf{p}|$ The quantities F_l^s and F_l^a are the spin–symmetric and spin–antisymmetric dimensionless Landau parameters

Properties of the Fermi liquid can now be calculated in terms of these parameters Since the Landau parameters must be determined from experiment, this is a semi–phenomenological theory The first few parameters can be related to simple measurements of the molar heat capacity C_N, speed of ordinary (first) sound c_1, and absolute magnetic susceptibility χ_N These relations are

$$C_N = \frac{m^*p_F}{3\hbar^3}k_B^2T \tag{2.11}$$

$$c_1^2 = \tfrac{1}{3}\left[1 + F_1^s\right]\left[1 + \tfrac{1}{3}F_1^s\right]v_F^2 \tag{2.12}$$

$$\chi_N = \tfrac{1}{3}\gamma^2\hbar^2N_F\left[1 + F_0^a\right]^{-1} \tag{2.13}$$

Also, m^* can be related to F_1^s by

$$\frac{m^*}{m} = 1 + \frac{1}{3} F_1^s$$

One of the most impressive accomplishments of the Landau theory that distinguishes it from a purely phenomenological theory is the prediction of collective modes due to the quasiparticle interactions In a temperature regime where the quasiparticle collision time , τ, is short compared to the characteristic period of an oscillating external force (a vibrating sound transducer), i e $\omega\tau << 1$, the quasiparticles can stay in equilibrium with the oscillations Thus is the so-called hydrodynamic regime and the propagating disturbance is ordinary or *first* sound As in classical hydrodynamics, the first sound propagation is determined by the compressibility κ, density ρ, and shear viscosity η The velocity is given by

$$c_1^2 = \frac{1}{\kappa\rho} \tag{2 14}$$

and the attenuation by

$$\alpha_1 = \frac{2\omega^2}{3c_1^3\rho}\eta \tag{2 15}$$

For the Fermi liquid, the compressibility is given by

$$\kappa = \frac{N_F m^2}{\rho^2\left(1+F_0^s\right)} \tag{2 19}$$

which is independent of temperature. The viscosity is

$$\eta = \tfrac{1}{5}\rho \frac{m^*}{m} v_F^2 \tau_\eta \propto T^{-2} \qquad (2.17)$$

so that the attenuation is proportional to T^{-2} in the hydrodynamic regime.

In the other extreme limit, $\omega\tau >> 1$, the quasiparticles cannot come into equilibrium in the time of one period. Ordinary sound, which relies on particle collisions for propagation, cannot be generated in this *collisionless* limit. In a Fermi liquid, however, the molecular fields (parameterized by the Landau parameters) that a quasiparticle finds itself in due to the other quasiparticles can react quickly enough to support a wave-like propagating mode. This mode in ^{3}He is excited and detected as longitudinal compressional waves and is called *zero sound*. This mode can be viewed as an asymmetric distortion of the Fermi surface.

To derive the relations for zero sound, one starts with the system in thermal equilibrium governed by the Fermi distribution

$$f_{\mathbf{k}}^0 = \left\{\exp(\epsilon_{\mathbf{k}}^0/k_B T) + 1\right\}^{-1} \qquad (2.18)$$

where $\epsilon_{\mathbf{k}}^0$ is the quasiparticle energy near the Fermi surface given by

$$\epsilon_{\mathbf{k}}^0 = \hbar^2 k^2/2m^* - \mu$$

With a time-dependent external disturbance on the system (compressional sound excitation), one can account for small deviations from equilibrium in the distribution function, $\delta f_{\mathbf{k}} = f_{\mathbf{k}} - f_{\mathbf{k}}^0$, as a linear functional of the disturbing field. Taking the exciting sound wave to have wave vector $\mathbf{q}$ and frequency ω, $\delta f_{\mathbf{k}}$ can be written in terms of its Fourier components

$$\delta f_{\mathbf{k}}(\mathbf{q},\omega) = \int d^3r dt\, \delta f_{\mathbf{k}}(\mathbf{r},t)\exp[i(\mathbf{q}\cdot\mathbf{r} - \omega t)] \tag{2.19}$$

The time evolution of these components is governed by the kinetic equation

$$\hbar\omega\delta f_{\mathbf{k}} - \epsilon_+^0 \delta f_{\mathbf{k}} + \delta f_{\mathbf{k}} \epsilon_-^0 + f_+^0 \delta\epsilon_{\mathbf{k}} - \delta\epsilon_{\mathbf{k}} f_-^0 = -i I_{\mathbf{k}}(\delta f'), \tag{2.20}$$

where the subscripts $\pm$ indicate $\mathbf{k} \pm \frac{1}{2}\mathbf{q}$ and $\delta\epsilon_{\mathbf{k}}$ is the change in quasiparticle energy due to the external field directly and that caused by a shift in the distribution function such that

$$\delta\epsilon_{\mathbf{k}} = \mathrm{Tr}_{\sigma'} \sum_{\mathbf{k}'} f_{\mathbf{k}\mathbf{k}'} \delta f_{\mathbf{k}'} + \delta\epsilon_{\mathbf{k}}^{\mathrm{ext}} \tag{2.21}$$

On the right side of equation (2.20) is the collision integral $I_{\mathbf{k}}$ that operates on the deviation from the local equilibrium distribution

$$\delta f_{\mathbf{k}'} = \delta f_{\mathbf{k}} - f_{\mathbf{k}}' \delta\epsilon_{\mathbf{k}} \tag{2.22}$$

where $f_{\mathbf{k}}' = \delta f_{\mathbf{k}}^0 / \partial\epsilon_{\mathbf{k}}$

The collective modes of a system appear as poles in the complex frequency plane of the corresponding response function such as the number density

$$\delta n(\mathbf{q},\omega) = \sum_{\mathbf{k},\sigma} \delta f_{\mathbf{k}}(\mathbf{q},\omega) \tag{2.23}$$

and the current density

$$\mathcal{J}(q,\omega) = \sum_{\mathbf{k},\sigma} \frac{\mathbf{k}\,\mathbf{k}}{m}\, \delta f_{\mathbf{k}}(q,\omega) \tag{2.24}$$

To obtain the longitudinal oscillation mode of the kinetic equation, eq (2.20), the conservation laws for particle number and momentum can be used. They are obtained from eq (2.20) through multiplication by the distribution function and k/m respectively and summing on k the results of this are

$$\omega\delta n = q\cdot\mathcal{J} \tag{2.25}$$

and

$$\omega\mathcal{J} = \sum_{\mathbf{k},\sigma} \frac{\mathbf{k}}{m}(\mathbf{v}_{\mathbf{k}}\cdot q)\delta f_{\mathbf{k}}' \tag{2.26}$$

where $\mathbf{v}_{\mathbf{k}}$ is the quasiparticle velocity, $\mathbf{v}_{\mathbf{k}} = \hat{\mathbf{k}}v_F$.

In the collisionless limit, the dissipation term in eq (2.20) can be set to zero. Landau (1957) showed that new propagating modes he called zero-sound could exist in this limit. For ^{3}He, all but the longitudinal sound mode are highly damped. The resulting relation for the zero-sound velocity in the extreme collisionless limit is

$$\frac{c_1 - c_l}{c_l} = \frac{2}{5}\,\frac{1 + \frac{1}{5}F_1^s}{1 + F_1^s} + \mathcal{O}\left(a_1^{-4}\right) \tag{2.27}$$

where

$$a_1^2 \equiv \left(\frac{c_1}{v_F}\right)^2 = \tfrac{1}{3}(1+F_0^s)(1+\tfrac{1}{5}F_1^s)$$

For ^{3}He, a_1^{-1} is negligibly small even at low pressures. It is this relation that is used

to deduce F_2^s from sound velocity measurements in this dissertation. The zero–sound attenuation is given by

$$\alpha_0 = \frac{2}{5}\frac{v_F^3}{c_1^3}\frac{1}{\tau_{\alpha}}\frac{m^*}{m} \qquad (2.28)$$

and has a T^2 dependence, the reciprocal of the first–sound results. Figure 2–1 shows the crossover from first to zero–sound through $\omega\tau=1$ of both velocity and attenuation from the data of Ketterson et al. (1975).

Sound in Superfluid ^{3}He

With the success of the BCS theory of electron pairing as an explanation of superconductivity (Bardeen, Cooper, and Schrieffer, 1957), many researchers applied this idea to the study of neutral Fermi systems. The combination of Landau's successful Fermi liquid theory for ^{3}He with BCS theory led to many predictions for the properties of a new type of "superconductor", superfluid ^{3}He. For many years, this new state of matter eluded experimentalists, with the estimated transition temperature always falling just out of reach of what was possible in the laboratory.

In 1971, refrigeration technology had finally reached the much sought after superfluid transition temperature (Osheroff et al., 1972). In the seventeen years since its discovery, superfluid ^{3}He has become a testing ground for a wide range of theoretical and experimental ideas in many–body physics. Several review articles are available on the subject. Two early and still valuable articles are a theoretical review by Leggett (1975) and an experimental review by Wheatley (1975). More textbook–like treatments can be found in the articles by Anderson and Brinkman (1978) and Richardson and Lee (1978).

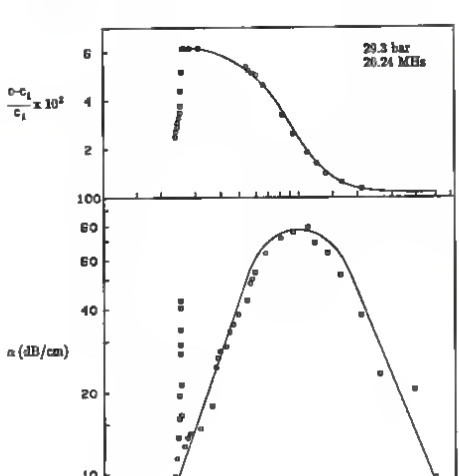

Figure 2–1 Zero–sound velocity and attenuation from Ketterson et al (1975)

One property of superfluid ^{3}He that has received intense study is its response to sound excitation. Because of the complex order of the superfluid state, many collective modes that couple to sound have been predicted and observed. A complete review of these phenomena can be found in an article by Wölfle (1978). For the restricted purposes of this dissertation, only the behavior of the sound velocity and attenuation, without effects due to the collective modes of the gap, will be discussed.

As discussed earlier in the section on the normal Fermi liquid, there are two distinct regimes for the propagation of sound. In the case of ordinary hydrodynamic sound, $\omega\tau \ll 1$, where ω is the sound frequency and τ is the quasiparticle collision time. Thus, for sufficiently low frequency, this regime extends all the way to the superfluid transition. Because the superfluid state is a result of correlations of the particles, the bulk thermodynamic properties should be unchanged from that of the normal liquid. Hence, the density, ρ, and compressibility, κ, should not change as the liquid is cooled through its transition and the hydrodynamic or first sound velocity should maintain its normal liquid value.

If the sound frequency is high enough, then the collisionless regime, where $\omega\tau \gg 1$, is entered in the normal liquid at low temperature. As described in the previous section, the propagating density wave, called zero–sound, is a result of the molecular field in which the quasiparticles find themselves. Now, when the superfluid is entered, the quasiparticles begin to pair up into Cooper pairs. These pairs no longer effectively behave as Fermions, hence, they do not contribute to the zero–sound restoring force. As the superfluid is cooled closer to T=0, the majority of the quasiparticles are paired up leaving no mechanism for zero–sound to be supported. As a result, there are no single quasiparticle states available for excitation and, hence, there is no dissipation. The fluid can now respond to density fluctuations at any frequency, as long as they are lower than the characteristic

frequency of the pairing, i.e. the gap frequency, $\Delta/\hbar$. At higher frequencies, the pairs are broken giving dissipative single quasiparticle excitations as in the normal liquid.

At temperatures near T=0, the superfluid, then, behaves as an ideal elastic fluid. The density wave that propagates remains in local thermodynamic equilibrium due to the quick response of the liquid, and, hence, behaves as first sound. Because the density and compressibility have not changed from the normal state, this low temperature mode should propagate at c_1. This prediction was first made in the context of neutral superconductors by Anderson (1958) and Bogoliubov et al. (1959). Wölfle (1973) has derived an expression for the full temperature dependence of the sound velocity below T_c using a generalization of the kinetic equation for normal Fermi liquids.

By the same argument as above, the lack of single quasiparticle excitations at low temperature reduces the sound attenuation. As the liquid is cooled into the superfluid, an attenuation peak is found near T_c, followed by a continuous drop as the temperature is decreased. The peak is attributed to the breaking of pairs by the sound quanta. Figure 2-2 displays the behavior of the sound velocity and attenuation in the superfluid without any excitation of order parameter collective modes.

Surface Magnetism of ^{3}He

Experimental Review

The question of how ^{3}He atoms behave at a surface has been studied for both pure and practical reasons for several years. The adsorbed layers of ^{3}He may represent a controllable two-dimensional nuclear spin system with quantum exchange that can be addressable by the quantum theory of magnetism. The enhanced relaxation of the spins at the surface has practical implications for the

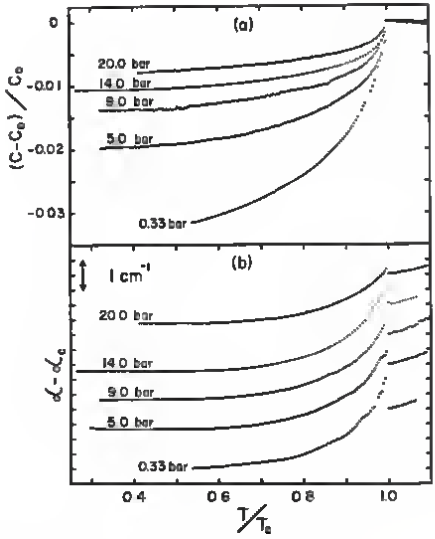

Figure 2–2 Ultrasound velocity and attenuation in superfluid ^{3}He–B from Ikas et al (1985)

understanding of heat transfer across a boundary at low temperature. This section will attempt to concisely review the voluminous amounts of measurements performed on ^{3}He confined in and adsorbed on many different substrates for the past twenty years. Unlike the previous section on sound, there is not at present a consistent theoretical picture for the mechanism of enhanced magnetism of helium atoms near a surface. One of the main impediments to theoretical progress is the uncontrolled and incompletely characterised nature of the various substrates used in the experiments, making it difficult to formulate a quantitative theory covering all of the data. This section will begin with a chronological description of the many experiments performed. Later, differences in the various systems will be explored.

Early NMR measurements on ^{3}He adsorbed on Vycor glass were performed by D F. Brewer's group at Sussex (Brewer, 1970). Their lowest temperature was a fairly high 400 mK, but they were able to see susceptibility contributions from individual layers of atoms in their experiment, the CW NMR signal was integrated to obtain the total susceptibility as controlled amounts of ^{3}He were added to the sample cell. Figure 2–3 shows the susceptibility as a function of coverage at T=0.405 K. The initial regime up to one monolayer, and possibly beyond, is linear, indicating that the addition of each spin has no effect with those already present. This is consistent with the idea that the first layer is a tightly bound high density solid in the Van der Waals potential and hence the spins are localized. Because the dipole–dipole interaction is on the order of 10^{-7} K, the spins do not interact at these temperatures. Thus, the susceptibility contribution of one layer is the classical Curie free–spin value ($\chi = C/T$) as evidenced by temperature dependence measurements of sub–monolayers between 0.4 and 1.2 K.

As higher layers are built up, the linearity disappears, and the susceptibility signal per added spin decreases. The authors interpret this as reflecting the onset of degeneracy. One important result to come out of these measurements can be seen

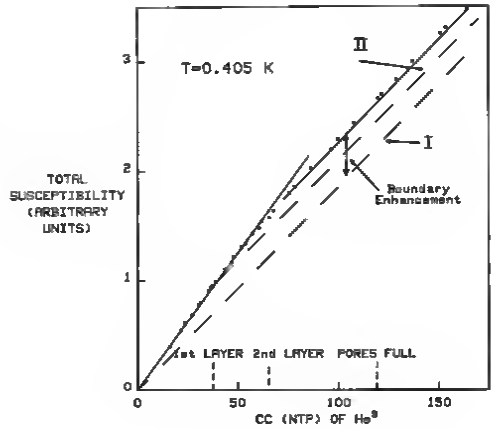

Figure 2–3 Susceptibility vs coverage of ^{3}He on Vycor adapted from Brewer (1970)

by comparing the susceptibility of the Vycor with filled pores to that of bulk liquid In figure 2–3, the dashed line labeled I is the susceptibility for plain bulk liquid while II is that for bulk liquid with the addition of just the first layer still behaving Curie–like The fact that the measured signal is above both of these lines indicates that the surface enhancement remains even though there is bulk liquid in contact with the outer layer This is not too surprising for the first layer because it is so tightly bound in the ~ 3K surface potential, but the second layer maintains its enhancement as well At this early point in these types of experiments, this *statistical layer model* was an adequate interpretation

The Sussex group performed another ^{3}He–in–Vycor experiment (Brewer and Rolt, 1672), this time filling the pores completely with liquid and cooling to ~ 50 mK Figure 2–4 is a plot of χT versus **T** at saturated vapor pressure This semi–logarithmic plot shows predictions for the bulk liquid and the statistical layer model previously introduced At these lower temperatures, the enhancement is greater than that for non–interacting layers This evidence for intra–layer communication is still very subtle at these temperatures, but clear enough that the simple picture of independent layers must be altered The surface contribution to the magnetism was seen to be Curie–like, however, because of the high minimum temperature, a Curie–Weiss dependence with a Weiss temperature of ~ 10 mK or less could not be ruled out One final very important effect was that upon introduction of ^{4}He in an amount equivalent to one layer, the excess magnetism completely disappeared This was interpreted as a displacement of the surface ^{3}He atoms by the more massive and therefore more tightly bound non–magnetic ^{4}He

It was not until an NMR experiment on superfluid ^{3}He in a parallel plate geometry was performed in Helsinki (Ahonen et al , 1676) that the temperatures were low enough to clearly observe the Curie–Weiss behavior of the spins on the surface of the stacked Mylar sheets The measurements were performed down to 0 7

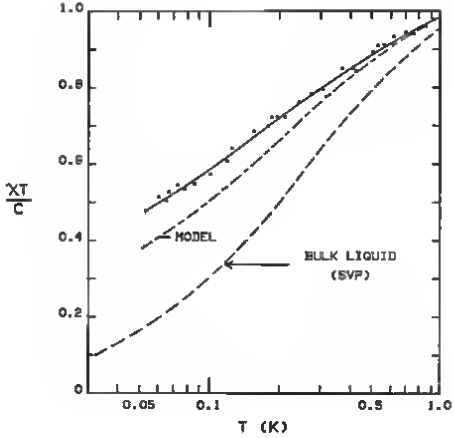

Figure 2-4. $\chi T/C$ vs T for Vycor with filled pores adapted from Brewer and Rolt (1972)

mK giving a Weiss temperature of ~ 0 5 mK Again, the effect disappeared with the addition of a sufficient amount of ^{4}He. This experiment prompted studies on other substrates cooled by nuclear demagnetisation The Helsinki group (Ahonen et al , 1978) performed pulsed NMR measurements on 90 Å carbon particles (Carbolac) immersed in liquid ^{3}He down to 0 4 mK. In the very small spaces between the particles, the superfluid could not form because the Cooper pair coherence length is larger than the wall distances This meant that the magnetic signal was not complicated by the complex magnetic nature of superfluid ^{3}He. They were able to separate out three different contributions to the susceptibility Because the first solid–like layer is assumed to be rather immobile, the free induction decay of the total signal would have a very quickly decaying component due to this solid. The carbon particle experiment showed a rapid decay of 40 μs preceding the slower decay of 400 μs in the FID The temperature dependence of the early time signal was consistent with a pure Curie law (they quote a Weiss temperature of –0 09 mK) while the larger long decay time signal was again a Curie–Weiss law with a Weiss temperature varying from 0 35 mK at 0 bars to 0 5 mK at 25 bars The third contribution was a temperature independent term attributed to a bulk–like degenerate Fermi liquid in the spaces between the particles

Another measurement made on this system was the apparent spin–spin relaxation time , T_2^*, which is actually a dephasing time of the precessing spins and depends not only on the microscopic relaxation processes, but on the overall magnetic field homogeneity As the temperature was lowered, T_2^* initially decreased but then began a rapid increase below ~ 2 5 K (see figure 2–5) The magnitude of this dephasing time was pressure dependent The authors interpret this low temperature increase as a ferromagnet approaching ordering This measurement is not, however, the intrinsic spin–spin relaxation time and may be subject to other effects to be discussed in Chapter 5 of this dissertation

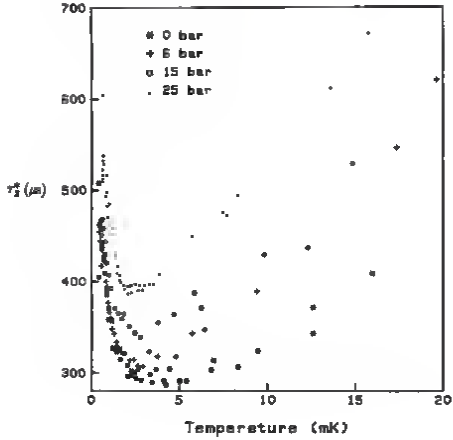

Figure 2–5 Spin dephasing time, T_2^*, vs T for liquid ^{3}He in 90 μm carbon particles adapted from Ahonen et al (1978)

At the time of the carbon particle experiment, the group at the University of Southern California performed NMR measurements on liquid ^{3}He in Grafoil (Bosler et al , 1978) Grafoil is an exfoliated graphite that is comprised of many atomically smooth platelets that are essentially parallel. Hence, the surface normal points in a unique direction relative to the external field unlike that of the randomly oriented carbon particles or the pores of Vycor glass Again, by cooling to 0 43 mK, a Curie–Weiss law with an extrapolated transition temperature of 0 36 mK was observed This time, however, a strongly magnetic field dependent susceptibility was seen As the field was increased, the enhancement was diminished, indicating that the external field energy is dominating the subtle interactions of the ^{3}He spins In addition, the spin dephasing time, T_2^*, was found to decrease as the temperature was lowered below 1 mK in contrast to that of the carbon particles One complication in this experiment was the fact that the Grafoil platelet spacing is still large compared to the superfluid coherence length Hence, the superfluid forms in the spaces, changing the environment the surface spins experience

Pursuing these measurements further, the USC group repeated the experiment on Grafoil a few years later (Bosler et al , 1983) The main results of this later experiment were the observation of an anisotropic frequency shift at low temperatures (see figure 2–6) and a very pronounced low temperature decrease in T_2^* The sign of the frequency shift depended upon the relative orientation of the external magnetic field with the surface normal of the Grafoil This was interpreted as indicating the true two–dimensional nature of the surface magnetic state. As the spins begin to order in a sheet, the local field determining the resonance frequency is the superposition of that from the external magnet and that from the helium spins. Hence, if the spins order in a particular direction that depends on the surface orientation and not on the external field, then the frequency will differ with the relative orientation of the field and surface normal vectors Also, the rapid

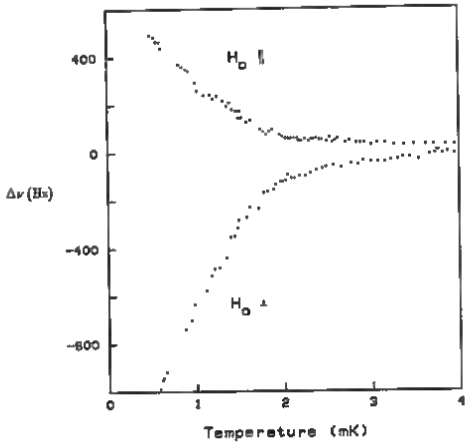

Figure 2–6 Field dependent frequency shift of ^{3}He in Grafoil adapted from Bonier et al (1983)

downturn of γ_2^e at low temperatures was interpreted by the authors as being evidence for two–dimensional behavior from theoretical predictions (Richards, 1976) for two–dimensional magnetic systems

In their recent work (Friedman et al., 1988), the USC group has pursued NMR measurements on the ^{3}He–Grafoil system in very low magnetic fields on the order of a few Gauss in order to be below the dipolar field energy of the interacting spins. Using very sensitive SQUID (superconducting quantum interference device) detection techniques, the authors have observed frequency shifted resonant modes at temperatures below the extrapolated Weiss temperature of 0.6 mK. They interpret these as resulting from collective modes within the ^{3}He surface layers ferromagnetically ordered over large domains. Thus, because the energy per spin in these low fields is 10^{-4} k_BT, this is direct evidence for large exchange–aligned domains.

One issue not addressed in the discussion so far is how many layers of atoms are causing this enhanced magnetism. The methods used to determine how much surface helium is present must obviously rely on a knowledge of the surface area of the substrate as well as how much of the surrounding helium the NMR coil probes. An accurate determination of this quantity is not easily obtained for the large surface–to–volume substances used as substrates. Also, the extent of the RF radiation from the probe coil can only be estimated. In addition, many times the dominant surface is that of the sintered heat exchanger making it difficult to determine where all of the helium actually plates out. These comments are, therefore, intended as a caution when comparisons between different experiments are made.

As mentioned earlier, the high temperature measurements on Vycor indicated two complete layers were responsible for the enhanced magnetism, the first being a high density solid and the second a high density liquid. Any additional

layers were found to behave as a degenerate Fermi liquid, albeit with a different Fermi temperature. In the carbon particle experiments, the authors used the ratio of the two different time constant contributions to the FID to estimate the amount of helium atoms involved. While they assumed a density and susceptibility of bulk solid ^{3}He for the long time constant signal, they obtained an estimate of 4.5 to 5.5 atomic layers. In the Grafoil experiments, the authors performed adsorption isotherms to obtain the surface area of the substrate. In addition, they determined the internal volume of the Grafoil so that the amount of liquid both inside and around the Grafoil could be calculated. Finally, they probed the distribution of the rf magnetic field at the end of the NMR coil and estimated that 40% of their signal was due to bulk liquid. Putting this all together, they estimate around 1 monolayer is responsible for the Curie–Weiss behavior.

It is clear that these determinations are only estimates. With the goal of accurately obtaining the number of layers responsible for the enhanced susceptibility, the Japanese group of Okuda et al. (1985) designed an experiment for such a purpose. The substrate chosen, though different from previous works and hence a new variable, was sintered Ag powder. In this way, the substrate could be cooled itself through conduction to very low temperature, eliminating the need for bulk liquid to be present as a thermal link. To avoid eddy current heating that would result from NMR measurements, the DC magnetization was measured directly via a SQUID magnetometer. This has the added complication of being sensitive to all magnetic materials present and hence a background measurement of the empty cell has to be performed and subtracted from the data. These workers found that for up to 5 layers of ^{3}He atoms, the behavior was Curie–like with no measurable Weiss temperature. When the coverage was increased beyond 5 layers, the behavior became Curie–Weiss with a Weiss temperature of 0.4 mK, consistent with the bulk liquid measurements.

In a recent measurement, the group at Grenoble (Franco et al , 1986) performed CW NMR on monolayers of ^{3}He on a Grafoil substrate down to 3 mK as a function of coverage Their striking results are shown in figure 2–7 The first one and a half layers obey Curie's law as seen before, with a very broad linewidth characteristic of a tightly bound solid When the coverage is increased, a peak in the susceptibility is seen at ≈2 5 layers. Hence, there is an optimal coverage for the enhanced magnetism, which can be exceeded The Weiss constant for the helium at this special coverage is a very high 2 9 mK and approaches the more usual 0 5 mK as the coverage is increased toward bulk liquid Hence, the existence of a layer above the first adsorbed layer is necessary for the ferromagnetism, but additional atoms can actually diminish the effect

Theoretical Review

There are at present several models described in the literature for explaining the surface induced ferromagnetism of ^{3}He. One of the earliest theoretical pictures (Beal–Monod and Domach, 1977, Spanjaard et al , 1979) views the effect as arising from a two–dimensional Fermi liquid that is driven near a ferromagnetic instability by the surface Van der Waals potential Two others treat the problem as being due to an exchange mediated magnetic interaction. Jichu and Kuroda (1982) view the dominant mechanism as an indirect exchange (RKKY) between two solid–like atoms within a layer which interact with a single liquid atom Delrieu et al (1980) attempt to account for the experimental data using direct three particle exchange within the solid layers Figure 2–8 is a representation of the different mechanisms involved in these models

Bulk liquid ^{3}He in the normal state displays an enhanced Pauli–like susceptibility when cooled well below its Fermi temperature (< 100 mK) The susceptibility for this Fermi liquid can be written

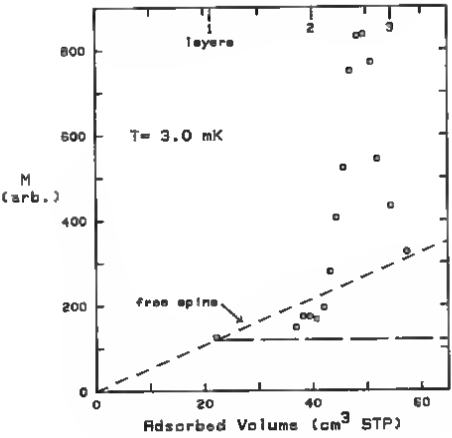

Figure 2–7 Magnetisation vs coverage of ^{3}He on Grafoil adapted from Franco et al (1986)

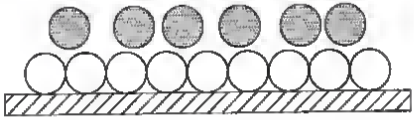

Ferromagnetic Liquid

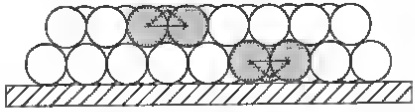

3–Particle Exchange

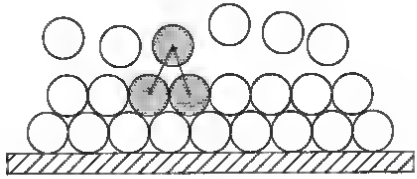

RKKY Exchange

Figure 2–8 Models for ^{3}He surface ferromagnetism.

$$\chi_{bulk}(T) = \chi(0)[1 - a\chi^2(0)T^2 + \ldots] \qquad (2.30)$$

where a is a constant independent of pressure The prefactor, $\chi(0)$, is the T=0 susceptibility that is enhanced over the value for the free Fermi liquid by roughly an order of magnitude The fact that bulk liquid ^{3}He is nearly magnetic in its natural state is the basis for the two–dimensional ferromagnetic liquid model introduced earlier (Bedl–Mourad and Doniach, 1977, Spanjaard et al , 1979) The basic idea of the model is that the Van der Waals surface potential increases the density of the quasiparticles in a thin sheet near the surface. This increased density is shown, in their calculations, to greatly enhance the magnetic response of the liquid adjacent to the surface.

Another approach, which was motivated by the qualitative success of the multiple spin exchange theory for bcc solid ^{3}He, was proposed by Delrieu et al (1980) Using geometrical arguments to determine which type of particle exchange would be favored for a triangular two–dimensional lattice, the authors conclude that the ferromagnetic tendency is produced by three particle exchange within the solid layers Because the magnetism is occurring in these first layers, this model is consistent with the destruction of the magnetic state with the addition of enough ^{4}He in a very recent paper, Roger and Delrieu (1987) state that the exchange frequency for the second layer is on the order of 1 mK giving a Weiss θ of a few mK This is in good agreement with the single layers on Grafoil experiment (Franco et al ,1986) In addition, the authors argue that the 2 5 layers required for the ferromagnetic peak in the experiment is a result of the final half layer localising the layer beneath Also, additional ^{3}He atoms are believed to increase the density of the under layers, thereby restricting the exchange and lowering θ

Jichu and Kuroda (1982) believed that the exchange constant for three particle exchange within a layer was an order of magnitude too low to account for

the surface ferromagnetism Their approach was to look at indirect exchange mechanisms between the solid atoms adsorbed on the substrate via the liquid in contact with the surface layer Following the formalism known as RKKY indirect exchange (Ruderman and Kittel, 1954, Kasuya, 1956, Yosida, 1957), they were able to account for the ferromagnetic tendencies of the surface atoms The spin-dependent Hamiltonian for interactions in the solid layer is written as

$$H_{ex} = -\sum_{i<j} J_{ij}^{(d)} \vec{S}_i \cdot \vec{S}_j \qquad (2\,31)$$

where $J_{ij}^{(d)}$ is the exchange constant This constant for direct exchange within a layer is estimated to be of order 1μK (Cowan et al , 1977) which is too small to explain the experiments Using a simplified model of a semi-infinite system of ^{3}He atoms bounded by a plane surface of a substrate, the authors calculate an exchange constant of

$$J_{ij}^{(1)} \simeq 0\,15 \text{ mK} \qquad (2\,32)$$

for nearest neighbor pairs via the RKKY interaction Since it is positive, it favors ferromagnetism The transition temperature is given by

$$T_c = \frac{aJ_{ij}^{(1)}}{2} \qquad (2\,33)$$

in the mean field approximation where a is the number of nearest neighbors This gives $T_c \simeq 0\,45$ mK for a triangular lattice, which is in good agreement with experiment

CHAPTER 3

EXPERIMENTAL APPARATUS AND TECHNIQUE

Refrigeration

The refrigerator on which the experiments of this dissertation were performed consisted of a $^3He/^4He$ dilution refrigerator that was designed and constructed at the University of Florida by Dr E B Flint and a copper nuclear demagnetization stage designed and constructed by Dr G G Ihas and his group Many details of the cryostat and its construction techniques may be found in the Ph D dissertation of Dr R F Berg (1983) from this laboratory

The dilution refrigerator has a no load minimum temperature of 10 mK and can cool the copper demagnetization bundle in a field of 8 Tesla to 24 mK within 3 days after magnetization The nuclear cooling stage is made up of ~7000 Allex insulated wires to prevent eddy current heating which is annealed into a close packed bundle providing ~60 moles of Cu in the main magnetizing field The main magnet is a compensated superconducting solenoid built by American Magnetics capable of a central field of 8.5 Tesla at 75 A

This cryostat is capable of cooling several cubic centimeters of liquid ^3He to minimum temperatures of ~0 25 mK, but its true strength is the enormous heat capacity the large copper bundle provides at low temperature Temperatures below 2 mK can easily be maintained for several weeks with a series of small demagnetizations which allows easy experimentation in the ^3He superfluid phases For the experiments discussed here, the minimum temperatures were desired though, however, some sacrifice in lowest temperature was made to insure a large

enough heat capacity to allow good thermal equilibrium in the sample as the system warmed under the residual heat leak Typically, the bundle was precooled to ~25 mK after magnetizing to 8 5 T The demagnetization began with a period of rapid current change at high temperature where the eddy current heating is less of a problem. This was done to conserve the liquid helium bath which is rapidly consumed by the heat generated in the normal metal magnet leads with high current in them Usually after this period a helium transfer was simultaneously performed to top up the bath so the system did not have to be disturbed at its lowest temperature. After about an hour after the demagnetization was begun the rate was slowed to 1/4 the initial value and the superconducting heat switch connecting the Cu bundle to the mixing chamber was opened This rate was continued for another ~12 hours at which time the NMR and sound were begun and the demagnetitization rate was slowed to the slowest rate of the power supply with ~10 % of the starting field on the bundle The magnet was persisted at 0 8 % of the 8 5 T initial field giving a theoretically reversible cooling of the copper to 0 14 mK In actual practice, the ^{3}He sample could be cooled to 0 3 mK

Experimental Cell Heat Exchanger

The above description of the refrigerator describes minimum temperatures attainable for cooling liquid ^{3}He, but makes no mention of the difficulties of making thermal contact to the helium Because the boundary resistance to heat flow is very high between ^{3}He and its container walls at low temperature, the approach to encourage heat transfer has been to maximize the surface area with which the helium is in contact This is accomplished with a heat exchanger consisting of an annealed high conductivity copper body packed with very fine metal powder. The exchanger body is then placed in good thermal contact with the demagnetizing bundle The resulting surface area is usually on the order of 10 m^2 allowing for

thermal time constants at low temperatures for bulk ^{3}He of ~6 min. For the two experiments in this dissertation, two different heat exchangers were used. Both were made to be interchangeable and bolted to the Cu bundle with gold–plated feet. One exchanger (the one for the Vycor experiment) was made of sintered Palladium from a recipe developed by G. Ihas and J. Landau (details available in Munthag, 1978). The other was constructed from cold packed silver powder by R. Berg (1983). Detailed comparison of various materials used for heat exchangers can be found in the article of Berg and Ihas (1984), but the main conclusion is that simple packed silver has the highest performance with the lowest effort of construction.

Thermometry

The thermometers used in these experiments can be divided into two regimes of application. The temperature range of 20 mK $< T <$ 300 K is covered by an assortment of carbon resistance thermometers attached to various parts of the refrigerator. The carbon resistor attached to the experimental cell itself lost sensitivity below ~ 20 mK and was calibrated against a Ge resistor (Lake Shore Cryotronics). Measurement of the resistances was by a two–terminal AC bridge (Linear Research model LR 130) with very low excitation power (pW) to avoid self–heating.

Below 20 mK, pulsed NMR measurements of the magnetic susceptibility of platinum (Pt) nuclei were used as a thermometer. The Pt has been shown to obey a Curie law well below the temperatures attainable in these experiments and so the susceptibility is inversely proportional to the temperature. The thermometer consisted of 0.8 gm of 1 μm Pt particles (Leico Industries, 99.95% purity) packed to a 50% packing fraction in a cylindrical epoxy coil former. The use of fine powder allows for low eddy current heating from the NMR rf pulse as well as good thermal contact between the Pt and the liquid ^{3}He. The NMR spectrometer is a commercial

dedicated instrument (Instruments for Technology PLM–3) that has only four operating frequencies Thus, the magnetic fields used in the experiments are dictated by these frequencies In the surface magnetism experiment to be described in a later chapter, the susceptibility of the ^{3}He could be used as a thermometer at fields not supported by the PLM–3. The Pt thermometer is only a relative measurement and must be calibrated against a known fixed point For this purpose, the ultrasound behavior of superfluid ^{3}He is used The attenuation of ultrasound undergoes a sharp step at the transition temperature, T_c and thus allows the Pt to be used relative to T_c In the ultrasound experiment, the necessary measurement apparatus was already present, however, for the Vycor experiment an additional sound cell was constructed to look at the bulk liquid By using T_c of the superfluid as a reference, all temperatures may be scaled at a later date if and when an agreed revision of the temperature scale is invoked This has already happened since the bulk of this dissertation data was obtained (Greywall, 1986) At the lowest temperatures, the eddy current heating in the Pt can become a problem so that the NMR cannot be pulsed too frequently In the Vycor experiment, where precise knowledge of the temperature was required, care was taken to not cause any thermal standoffs The Pt NMR was performed once every fifteen minutes and fired just prior to the ^{3}He NMR pulse This combination assured no interference, either thermally or electronically, between the two probes

In the ultrasound experiment, the Pt susceptibility was recorded versus time as the experiment warmed monotonically under the residual heat leak High order polynomial fits were then performed on the data to reduce the scatter, and the resulting curve then converted to temperature versus time for use with the ultrasound data

Ultrasound Techniques

The electronic system for the measurement of ultrasound is schematically illustrated in Figure 3–1. The method was that of pulse transmission through the medium of interest (liquid ^{3}He) where both attenuation and phase velocity changes of the received pulse are measured simultaneously.

The x–cut quartz transmitting crystal is driven at its fundamental resonant frequency of 5 MHz via the amplified and gated output of PTS 200 synthesizer. The rf power amplifier used was a Matec 310RF which was triggered at 30 Hz synchronously with the 125 VAC line. The resulting output, 10 cycle bursts of 5 MHz RF coherent with the pulse envelope, was attenuated to a peak–to–peak amplitude of 0.6 volts before being applied to the sound transducer. The signal excited in the receiving transducer is first amplified by a doubly tuned preamplifier (Matec 252) and then by a 200 MHz wideband amplifier (Matec 625). The signal was then split, one half going for attenuation measurement and the other for phase change measurement.

To measure the signal amplitude (and hence attenuation) the received RF signal was sent through a compensated detector (Model 625 Matec) and then signal averaged 4000 times in a digitizer (Nicolet 1170). The digitized signal was then transferred to a computer (Hewlett–Packard 9845A) via RS–232 where ample analysis was performed. The baseline at late received times was determined from an average of the last 100 points and subtracted to account for any drift in the electronics. The amplitude of the signal could then be determined at any desired time within the received sound pulse which proved to be important in the understanding of observed attenuation satellites in superfluid ^{3}He–B to be described in Chapter 4. Generally, for the determination of attenuation, the signal height on the leading edge of the received signal just before the peak was used. To determine the attenuation, the amplitude was scaled relative to that at a reference

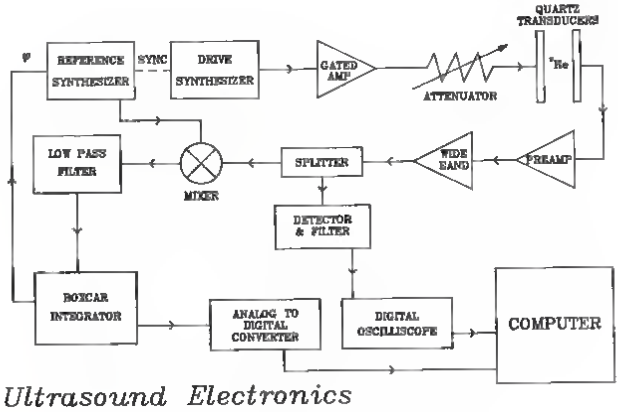

Figure 3–1 Ultrasound detection electronics

temperature (T_c of the superfluid) thus giving

$$\alpha - \alpha_c = \frac{1}{l} \ln\left[\frac{A_c}{A}\right] \qquad (3.1)$$

where l is the cell path length, A_c is the the amplitude at T_c and α is the attenuation defined as $A = A_0 e^{-l\alpha}$.

For phase velocity measurement, a variation of a feedback technique developed by R.F Berg (1983) was used. The other half of the split RF signal was mixed with a 5 MHz reference sine wave supplied by an HP 3325A synthesizer. The output of the doubly balanced mixer is the product of the two inputs which can be written as

$$A(t) = \left[A_s \sin(\omega_s t + \varphi_s)\right]\left[A_r \sin(\omega_r t + \varphi_r)\right] \qquad (3.2)$$

where A_x, ω_x, and φ_x are the amplitude, frequency and phase of the two input signals and the subscripts s and r are the sound and reference respectively. Now, for this experiment the frequencies of the two signals are the same, so with trigonometric manipulation this can be rewritten as

$$A(t) = A_s A_r\left[\frac{1}{2}\cos(\varphi_s - \varphi_r) + \frac{1}{2}\cos(2\omega t + \varphi_s + \varphi_r)\right] \qquad (3.3)$$

where the first term is a DC voltage dependent on the desired phase difference. The second term is oscillating at twice the operating frequency and is easily filtered out with a low pass filter.

Since this was a pulsed measurement, the above DC voltage is only as long as the received sound pulse. The amplitude of this signal was measured with a boxcar

integrator (Princeton Applied Research CW-1) with a gate time coincident with the pulse. The output of the boxcar is thus proportional to the cosine of the relative phase of the sound signal and reference. This output has the opposite polarity and so can be used as the error signal in a feedback loop to modulate the phase of the reference oscillator as shown in Figure 3-1. To analyze this high gain phase-locked loop, the output of the boxcar is just

$$V_0 = -gV_i \tag{3.4}$$

where g is the gain. If this voltage is then used to modulate the phase of the HP synthesizer, then

$$\varphi_r = aV_0 + \varphi_0 \tag{3.5}$$

where φ_0 is a constant and a is the gain factor for phase modulation in the synthesizer. Placing these expressions in equation (3.3) with the oscillatory term filtered out gives

$$\frac{V_0}{g} = \frac{A_s A_r}{2} \cos\left[\varphi_s - aV_0 - \varphi_0\right] \tag{3.6}$$

Now, if the loop is locked, V_0, and hence V_0, is kept near zero, so the above cosine can be expanded and after some algebra

$$V_0 = \frac{\frac{A_s A_r}{2}\left[\varphi_s - \varphi_0 - \frac{\pi}{2}\right]}{\left[\frac{1}{g} - \frac{A_s A_r}{2a}\right]} \tag{3.7}$$

Because the loop is high gain, $\frac{1}{g}$ can be ignored to first order so the final expression is

$$V_0 = -\frac{1}{k}\left[\varphi_s - \varphi_0 - \frac{\pi}{2}\right] \tag{3.8}$$

which is linear in the phase change of the sound signal. From the above relation, it is clear that higher order corrections involve the signal amplitude. To account for this amplitude dependence, calibrations were performed at fixed temperature by monitoring the phase measurement as the power of the transmitter pulse was varied in 3 dB steps. Then, in the later analysis of the phase versus temperature data, the effect could be removed by using the simultaneously obtained sound amplitude data. The corrections were never more than 5% in the worst case for the sound velocity.

NMR techniques

For the surface magnetism of ^{3}He in Vycor experiment, pulsed NMR was used for the bulk of the measurements. On one occasion, continuous wave (cw) NMR was used to observe the lineshape of the ^{3}He as a function of temperature. This section will discuss both of the setups and techniques for these differing methods.

The schematic of the circuit used for the pulsed NMR is shown in figure 3–2. The method is very similar to that used in the ultrasound measurements already discussed in that it involves an rf power amplifier gated in short pulses to provide excitation to the sample and a sensitive rf receiver to amplify the weak coherent signal induced in the probe coil by the precessing spins. The main difference, and hence difficulty, is that the desired signal begins immediately after the application of the transmitter pulse unlike in ultrasound where there is a propagation delay. Whereas in ultrasound one is always plagued by unwanted feedthru affecting the

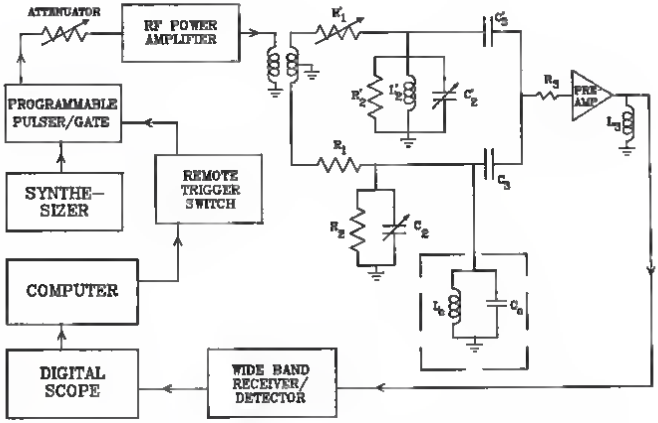

Figure 3–2. Pulsed NMR spectrometer

receiving electronics, in pulsed NMR, the transmitter pulse is applied directly to the same coil used for detection. Hence, this large voltage pulse would wreak havoc with the sensitive signal amplifier if it is not eliminated first.

Many approaches to the elimination of the transmitter pulse from the receiver have been developed through the years (Fukushima and Roeder, 1981). A simple and effective solution is that of the dummy cancellation circuit shown in figure 3–4. A bridge circuit using an rf center–tap transformer (Mini Circuits MCL T4–1) splits the rf pulse into two 180° out of phase components. Half goes to the NMR probe tank circuit in the cryostat and half goes to a dummy tank circuit that matches the low temperature one as nearly as possible. The output of the two tank circuits is recombined before sending it to the receiving electronics. When the bridge is precisely balanced, the transmitter pulse is canceled out almost completely thus leaving the receiver unperturbed and ready to amplify the NMR signal. When the excitation stops, the bridge is unbalanced and the receiver sees only the NMR tank circuit. This technique works well for the true oscillatory portions of the rf pulse where the two tank circuits are tuned to a narrow frequency, however it does suffer from the transients of the pulse. Generally, the first usable signal was $\lesssim 100$ μs after the pulse due to recovery of the amplifier and depended on the drive power. At the lowest temperatures, where the NMR signal is the strongest, smaller pulses were used and the dead time was therefore much reduced.

The rf power amplifier used (ENI model 403L) was capable of 30 V p–p output. A synthesizer (HP 3322A) tuned to the Larmor frequency at the particular field supplied the radio frequency energy and was gated into pulses via a locally built digital pulse programmer (Larry Frederick, staff electronics engineer). The pulser utilizes the input rf itself as a clock and therefore counts the number of cycles desired for a given pulse. These pulses are thus coherent with the excitation rf. The rf switch used as a gate has the capability of sending out pulses of differing

amplitudes allowing the programmer to output pulse sequences of various timings, lengths and heights For the Vycor experiment described here, two modes of operation were used For magnetic susceptibility, χ, and transverse dephasing time, τ_2^*, determination, single pulses were used and the Free Induction Decay (FID) recorded. For measuring the longitudinal relaxation time, τ_1, one large 90° pulse and fifteen ≈5° sampling pulses were used The small pulses monitor the magnetization recovery toward the Z axis and show an exponential growth of their corresponding FIDs with a time constant τ_1 (more details of the physical results is given in chapter 5)

The resulting NMR signals were first preamplified (60 dB Analog Modules) and then sent to a 200 MHz wide band receiver (Matec model 605) with only its second stage amplifier used It was found that the first stage degraded the signal to noise ratio (a design limitation to increase the bandwidth) and was not needed due to the strong ^{3}He signal Because the digitising rate of our signal averager (Nicolet 1170) was incapable of effectively capturing the raw oscillating FID, the NMR signal was first sent through a compensated detector (built into the Matec 605) to provide just the decaying envelope to the digitizer The digitized envelope was then transferred to the computer (HP 9845a) for analysis This technique provided no problems for a majority of the data accumulated, however, at high temperature where the signal size is very small, nonlinearities in the detector adversely affect the small amplitude tail of the decaying FID thus throwing off the computer fits The problem could usually be avoided by an appropriate boost of power, and only occurred in a small amount of data above 1 K

The dummy cancellation technique can be employed to improve the signal to noise ratio in continuous wave NMR. A schematic of the electronics for this setup is shown in figure 3–3 This spectrometer uses a high frequency lock–in amplifier (Princeton Applied Research, model 5202) for phase sensitive detection A vector

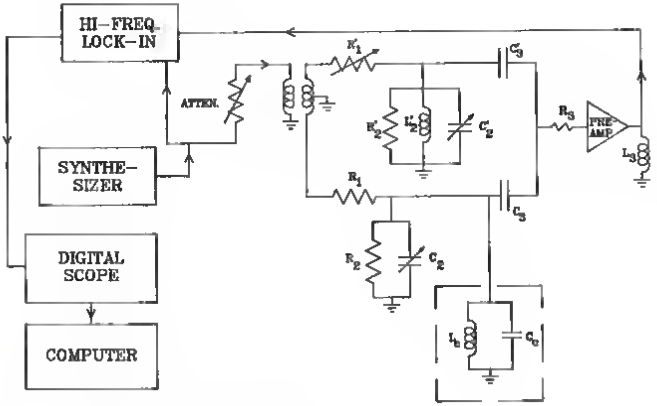

Figure 3–3. Continuous wave NMR spectrometer

summing circuit built into the lock-in provides magnitude information, independent of phase shifts The dummy circuit is adjusted to provide extinction of the rf when off resonance, thus allowing a higher sensitivity setting on the lock-in. When the field is swept through resonance, the out of balance signal is detected.

Experimental Cells

Details of the experimental cells used appear in the dissertations of their builders (R.F Berg (1983) for the Ultrasound cell and G F Spencer (1986) for the Vycor cell). In this section, enough cogent details of the cell design will be given to enable the reader to understand the results of the different experiments

A schematic drawing of the ultrasound cell is shown in figure 3-4 The main features necessary for the experiment described here are the sound cell and compressor The sound cell consisted of two 0 375" diameter gold plated quartz transducers of 5 MHz fundamental resonance frequency separated with a 6 25 mm epoxy spacer The spacer provided only four small contact points for each transducer to reduce sound transmission through the epoxy and was coated in silver paint and grounded to aid in shielding The relatively low frequency of the transducers was a drawback in the sound velocity determination of F_2^n in this experiment, but was a result of design considerations for the original purpose of the cell as a probe of solid ^{3}He These limitations were overcome as described in chapter 4

The other important feature is the variable volume nature via the ^{4}He driven bellows compressor Though designed with solid ^{3}He crystal growing in mind, this feature allowed high precision pressure regulation to be performed which turned out to be very important for the velocity measurements in liquid ^{3}He due to its strong dependence on pressure. Figure 3-5 shows a schematic of the feedback system for pressure regulation The pressure was monitored with a beryllium-copper strain

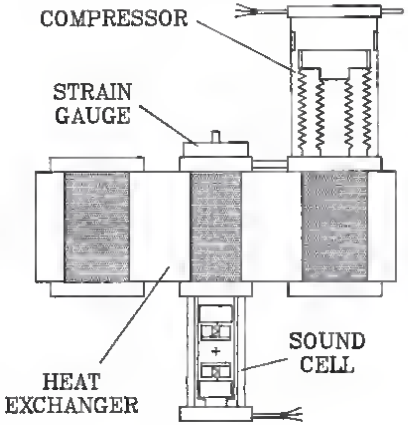

Ultrasound Apparatus

Figure 3–4. Ultrasound experimental apparatus

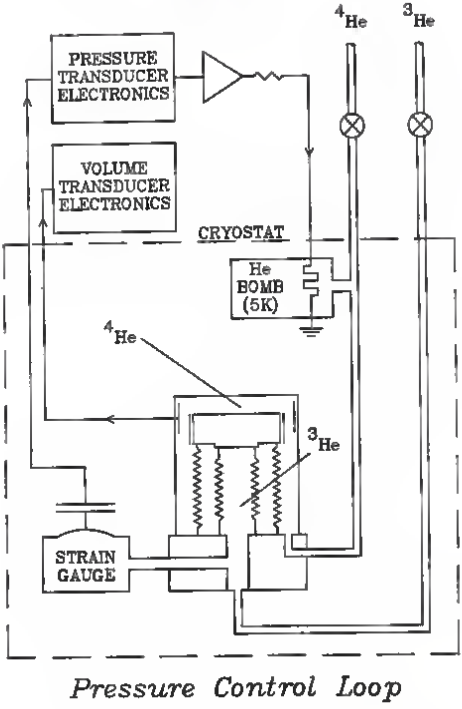

Figure 3–6 Pressure control feedback loop

gauge of the design made famous by Straty and Adams (1969) The output of the strain gauge bridge was used as the error signal for a temperature controller whose heater current was supplied to a bomb of ^{4}He weakly thermally connected to the 4 2 K bath Hence, the bomb pressure drove a bellows of liquid ^{4}He which in turn controlled the volume of the ^{3}He cell With this arrangement, the pressure was stabilized to better than 1×10^{-5} As an aside, this arrangement was also used via computer control to perform controlled growth of solid ^{3}He where the feedback parameter could be time, volume or the NMR susceptibility of the growing solid.

The Vycor cell was of a fairly complicated design which allowed several different probes to be used on the system (see figure 3–6) The main purpose was for sensitive flow studies of liquid through the Vycor A bellows pump designed and built by E Flint and G Ihas was described in detail in the dissertation of G Spencer (1986) and was used only for one small part of the data presented in this dissertation Complimentary to the pump was a very sensitive differential manometer designed by G Spencer It turned out that the manometer was actually a drawback for this experiment because it did not allow pressures above 9 bar to be studied The experimental cell also contained a pair of quartz ultrasound transducers to monitor the bulk liquid attenuation for use as a secondary thermometer in addition, two NMR coils were included for measurement of the confined ^{3}He and the susceptibility of platinum powder for thermometry

Important for the experiment performed for this dissertation was the placement of the saddle–shaped NMR coil on the Vycor rod itself. This coil only probed the center of the rod (see Figure 3–7) and the entire assembly was imbedded in Stycast 1266 The liquid ^{3}He was supplied to the ends of the Vycor rod via 1/8" tubes thereby enabling the NMR coil to only probe the ^{3}He confined in the glass making subtraction of a bulk signal unnecessary in the analysis With this cell, NMR and flow could be performed simultaneously and resulted in some interesting

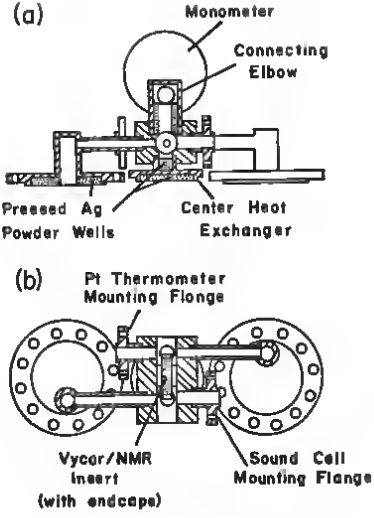

Figure 3–6. NMR and flow of ^{3}He in Vycor cell.

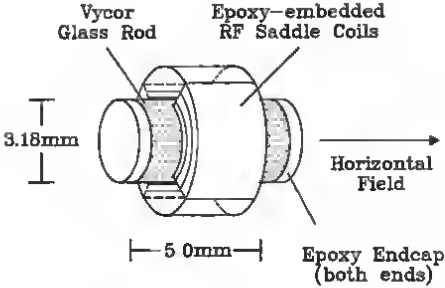

Figure 3–7 Detail of Vycor rod with RF saddle coils

effects discussed in Chapter 5

Data Aquisition

Both of the experiments performed were monitored with a Hewlett–Packard 9845A microcomputer. The computer was used in a passive data logger capacity instead of as an active controller of the experiment to keep inherent noise generated by its digital circuitry out of the sensitive low temperature environment. This was accomplished by having all analog outputs from the sensitive measuring electronics sent through the shielded room wall via low pass filters. The dc voltages resulting from the lock–in amplifiers and the boxcar integrator were measured with a multichannel analog–to–digital scanner (HP 3421A) which could be read via GP–IB by the computer. The scanner has a computer controllable–switch which allowed the computer to fire the ^{3}He NMR at preselected times branching the data logging program into its measurement subroutine. Another nice feature of this automated data aquisition system was a remote access capability from a home computer with a modem. This allowed for late–night peace of mind by transmitting the last ten data points when called up. As a safety measure, this remote feature allowed no active control of the host computer, but merely caused a data dump subroutine to be invoked when the modem connection was made. Because of the vintage and hence questionable reliability of the lab computer (purchased in 1978) this feature saved several data sets from oblivion.

CHAPTER 4

ULTRASOUND RESULTS IN LIQUID ^{3}He

Introduction

This chapter presents measurements of ultrasonic attenuation and velocity in normal and superfluid ^{3}He which will then be compared with the Landau theory of Fermi liquids and used to determine the second symmetric Landau parameter, F_2^s. First, an explanation of spurious attenuation satellite peaks in superfluid ^{3}He–B, first reported by Paulson and Wheatley (1978), and a method for their removal will be presented.

Identification of attenuation satellites

Ultrasonic attenuation and velocity were measured in liquid ^{3}He as a function of temperature and pressure by pulsing 5 MHz quartz piezoelectric crystals in a variable volume cell described earlier. The pressure of the ^{3}He was monitored with a beryllium–copper capacitive strain gauge and used in a feedback loop to regulate the pressure by varying the volume of the cell. This was accomplished with a dual bellows compressor using a ^{4}He filled drive bellows connected to a bomb with a heater controlled by the pressure measuring feedback loop (see chapter 3). This setup allowed the pressure to be regulated to within 1×10^{-5} and hence, due to the strong pressure dependence of the ^{3}He sound velocity, provided an increase in the precision of the velocity determination.

The measurements were made by propagating 2 μs long pulses of coherent 5 MHz tonebursts between two X–cut quartz crystals. The helium sample was

defined by an epoxy spacer with a cold length of 0.25 mm and 5.0 mm inside diameter separating the two quartz transducers. The amplitude and phase relative to a reference oscillator were measured from the first received sound pulse, thus giving the relative attenuation and phase velocity of the ^{3}He. This is ordinarily a very straightforward technique, however, unusual attenuation peaks were seen in this experiment and needed to be understood and accounted for to obtain the true behavior of the ^{3}He.

As liquid ^{3}He is cooled through the superfluid transition, the expected behavior (see chapter 2) for ultrasound attenuation at this frequency is a large absorption peak at T_c due to pair breaking and then a monotonic decrease to an asymptotic value at T=0 (this does not include the known collective modes which are obscured in the pair breaking peak at this low frequency). Figure 4-1 shows the raw amplitude as a function of temperature for this experiment. The unusual oscillations seen are similar to those first reported by Paulson and Wheatley (1978) and later seen by other workers (Giuretta, 1980, Meisel, 1983). The peaks are equally spaced when plotted versus $(1-T/T_c)^{1/2}$ in all of the experiments where they are seen, but the number of the peaks and their absolute spacing differs. Obviously, a spurious apparatus dependent effect is disturbing the measurement and must be accounted for.

In all pulsed ultrasound experiments, the exciting transmitter pulse is usually on the order of volts in amplitude. At the same time, the receiver circuitry is sensitive to the small voltage fluctuations of the piezoelectric crystal and thus can easily pick up stray electromagnetic energy from the transmitter. This so called *feedthru* signal is always present and efforts to minimize it are made by proper shielding. In the case of this experiment, this feedthru signal causes a persistent ringing in the receiver that is present when the actual transmitted sound pulse arrives. The effect of this mixing is most clearly visualized as a vectorial sum of

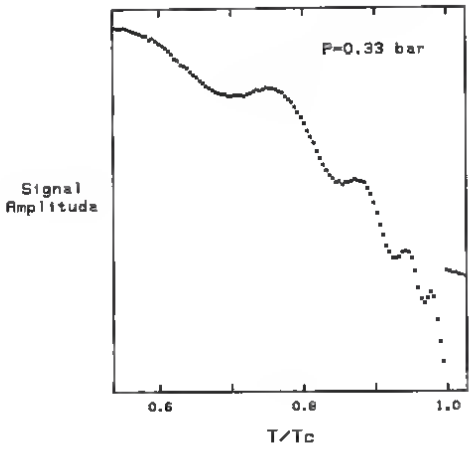

Figure 4–1. Raw zero–sound amplitude below T_c

phasors rotating at frequency ω (see figure 4–2) The magnitude, D(T), of the resulting detected signal is given by

$$|D(T)| = |A(T)|^2 + |C|^2 + 2|A(T)||C|\cos\varphi(T) \qquad (4\,1)$$

where A is the pure ^{3}He sound signal, C is the electromagnetic feedthru signal, and φ is the relative phase angle between A and C The temperature dependence of the interference term is due solely to the variation of the sound velocity and the attenuation of the ^{3}He below T_c, since the amplitude, C, and phase of the electromagnetic signal are independent of temperature This term produces one undulation (or maximum) on the detected signal whenever $\varphi(T)$ varies by 2π as the sound velocity changes with temperature. Since at a given pressure this velocity has a roughly $(1-T/T_c)^{1/2}$ temperature dependence, the undulations are approximately evenly spaced on such a temperature scale. The phase change, however, is dependent on the sound path length and frequency causing the maxima spacings to be apparatus dependent For different sound–cell configurations, the phase changes are related by

$$\Delta\varphi = (l/l_0)(\nu/\nu_0)\Delta\varphi_0 \qquad (4\,2)$$

where l and ν are the sound path length and frequency, respectively For the path length of 6 25 mm in this experiment compared to Paulson and Wheatley's length of 12.7 mm, at identical frequencies, half as many satellites with approximately twice the spacing were observed Using our simultaneously performed velocity measurements to obtain the phase angle changes and scaling with the above relation, these peak positions correspond to those of Paulson and Wheatley to within 0 2%

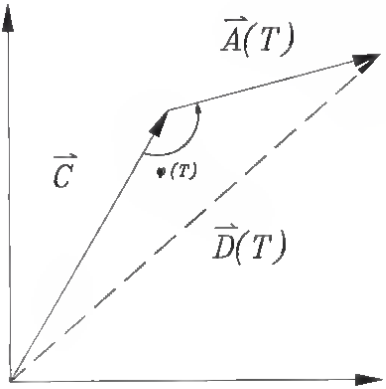

Figure 4–2. Phasor representation of coherent addition of feedthru signal

Now, because the root of the effect is understood, it is possible to independently measure enough parameters in equation (4.1) to determine the actual signal amplitude, $|A(T)|$, and hence the actual attenuation. Simultaneous phase change measurements using a high gain phase-locked loop (described in Chapter 3) provided $\varphi(T)$. To obtain $|C|$, the magnitude of the feedthru signal, it is only necessary to bring the ^{3}He to a temperature such that $\omega\tau \gg 1$, where ω is the sound frequency and τ is the quasiparticle collision time. In this regime, ordinary first sound cannot propagate and the collisionless limit for zero sound is not yet attained. So, no sound propagates through the ^{3}He and all that is received is the feedthru signal C. As a verification of the temperature independence of C, it can be measured at low pressure at the attenuation maximum of the superfluid near T_c where it is found to be constant for this factor of ~10 in temperature. Figure 4-3 shows the amplitude of the received sound pulse as a function of temperature both before and after the removal of the interference effect showing the true monotonic behavior of the superfluid ^{3}He-B attenuation as $T \to 0$.

Figure 4-4 is a plot of velocity and attenuation relative to the values at T_c versus T/T_c for five pressures. The monotonic behavior below the attenuation peak near T_c is theoretically expected (Wölfle, 1978). Both quantities approach temperature independent asymptotes by $T/T_c = 0.4$. These asymptotic values can now be compared with theoretical predictions for the fully developed superfluid condensate (see Chapter 2).

Velocity Measurements as T→0

The relative velocity change is measured as a change of phase of the received pulse as compared to a reference. Thus, it is not an absolute measurement with this technique and must use an independent determination of the velocity as a calibration. The data displayed in Figure 4-4 is plotted as $\left[\frac{c-c_0}{c_0}\right]$ versus T, where

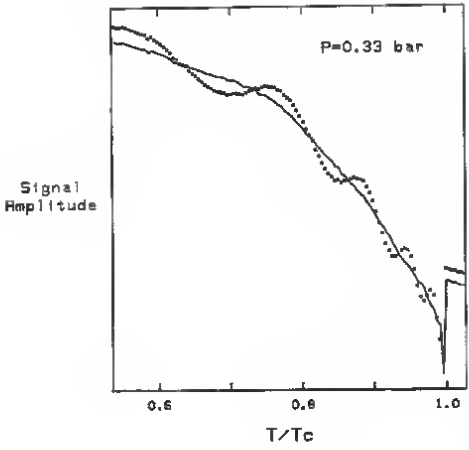

Figure 4–3 Zero–sound amplitude below T_c. Raw (points), interference removed (curve)

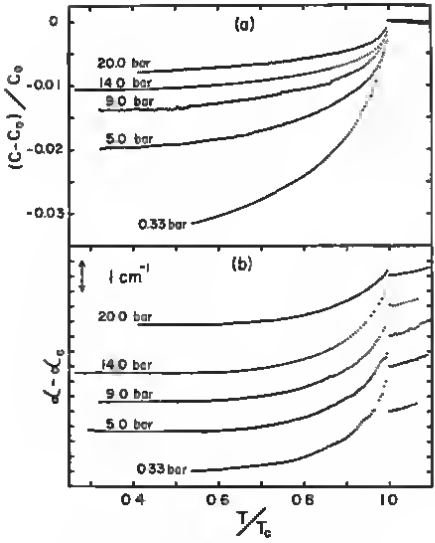

Figure 4–4 Zero–sound velocity and attenuation vs T/T_c

c_o is the zero sound velocity at T_c. This is convenient when one is interested in the behavior in the superfluid; however, measurement relative to the ordinary first sound velocity, c_1, facilitates more direct comparisons to the Landau Fermi liquid theory. To do this, the phase of the sound pulse must be tracked continuously from the temperature independent first sound region at high temperature, through the changeover to zero sound when $\omega\tau=1$, and finally through T_c into the low temperature asymptote (see figure 2–1). As mentioned earlier, the sound signal is lost in the high attenuation region where $\omega\tau=1$ and just below T_c; however, when the phase–locked loop arrangement unlocks, it always re–locks within a multiple of 2π when the signal returns. Thus, it is not difficult to keep track of the change in velocity over the entire temperature range because the overall behavior of the sound is already known.

With the velocity measured relative to c_1, comparisons with theory can be made. One prediction is that the velocity of zero sound in the fully developed superfluid condensate will return to the hydrodynamic value as a result of the zero temperature density mode (see Chapter 2). Figure 4–5 shows the zero–temperature asymptotic velocity relative to c_1 plotted against pressure. The velocity was found to approach c_1 within the experimental precision. Note that the error in these points is greater than the 1 part in 10^5 capability of the measurement system. This is mainly due to the measured voltages proportional to these velocities being very near zero. At 0.32 bar the sample did not cool fully into the asymptotic region so that an extrapolation was necessary, resulting in increased error. In addition to confirming the above theoretical prediction, because the velocity is identical to that of first sound in the normal Fermi liquid, the bulk compressibility and density thus remain constant to zero temperature, in spite of the intervention of the superfluid phase.

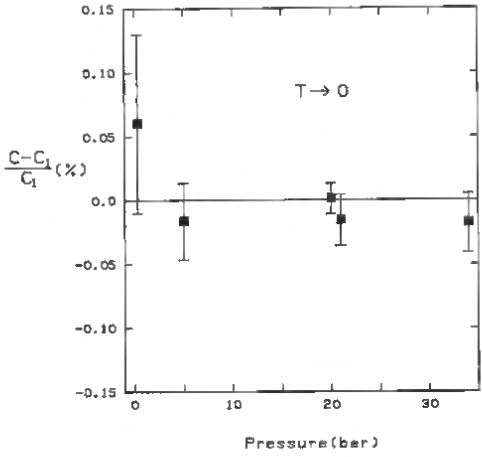

Figure 4–5 Percent difference between first sound velocity (c_1) and T=0 asymptote.

Pressure Dependence of F_2^s

The second symmetric Landau parameter, F_2^s, can be deduced from the difference in first– and zero–sound velocities. If higher order Landau parameters are ignored (see Chapter 2), then

$$\frac{c_0^2 - c_1^2}{c_1^2} = \frac{4}{5}\left[\frac{1 + \frac{1}{5}F_2^s}{1 + F_0^s}\right] \tag{4.3}$$

where F_0^s is the $l=0$ symmetric Landau parameter obtained from other experiments. Pure zero sound is realized in the limit $\omega\tau >> 1$. Thus, for sufficiently high frequency the zero–sound velocity, c_0, can be measured in the normal liquid just above T_c. However, for the 5 MHz sound used in this experiment, at T_c and high pressure this is not the case (e.g. at 34 bars $\omega\tau \approx 3$). Therefore, the velocity at T_c is somewhat less than c_0 and corrections for finite $\omega\tau$ must be invoked. For arbitrary frequencies the velocity of sound is given by (Wölfle, 1978)

$$c = c_1 + (c_0 - c_1)\mathrm{Re}\xi(\omega), \tag{4.4}$$

where

$$\xi(\omega) = (1 + i/\omega\tau_\alpha)^{-1},$$

and τ_α is the characteristic relaxation time for sound attenuation. The desired difference in the zero– and first–sound velocities may be then written

$$\frac{c_0 - c_1}{c_1} = \left[\frac{c - c_1}{c_1}\right]\left[1 + \frac{1}{(\omega\tau_\alpha)^2}\right], \tag{4.5}$$

where c is the actual measured velocity. This correction is greatest at the melting

pressure where it is ~12 % and insignificant at low pressure where is ~0 1 % The value of $\omega\tau$ at T_c as a function of pressure was obtained from $\tau_\eta T^2$ data tabulated by Wheatley (1975) where τ_η is the characteristic relaxation time for viscosity Though this is not the true quantity in the above expression, there is a very great lack of data on τ_α Comparisons of τ_α measurements (Abel et al , 1966, Paulson et al , 1973, Ketterson et al , 1975) with those of τ_η show them to be equal to within 5%, but because the τ_η data completely cover the full pressure range they were used in the correction in place of τ_α

Because the velocity was found to return to c_1 at the lowest temperatures in the superfluid, the precision in the determination of F_2^s could be increased by taking the phase difference from this asymptote and that at T_c to obtain $(c_0 - c_1)/c_1$ Figure 4–6 is a plot of $(c_0 - c_1)/c_1$ vs pressure The points are the measurements corrected for finite $\omega\tau$ and the curve is the theory with $F_2^s=0$ and F_0^s as scaled by specific–heat measurements of Greywall and Busch (1982) Thus, the deviation of the points from the curve is a measure of F_2^s

Figure 4–7 is a plot of F_2^s vs pressure The points are the determinations from this experiment as given by equation (4 3) The curve is a least–squares fit that has no actual physical motivation, but is given as an aid in calculations involving F_2^s This fit is a cubic in $P^{1/2}$

$$F_2^s = -1\ 284 + 0\ 896\ P^{1/2} - 0\ 167\ P + 0\ 0163\ P^{3/2} \qquad (4.6)$$

Figure 4–8 is a plot of F_2^s as calculated from these velocity data, but using the older values of F_0^s found in the Wheatley review article (1975) This was done to facilitate comparison with previous determinations of F_2^s, but it also shows the sensitivity of F_2^s to m^*/m determinations As can be seen, good agreement is found with earlier work in which F_2^s was obtained from longitudinal velocity measurements

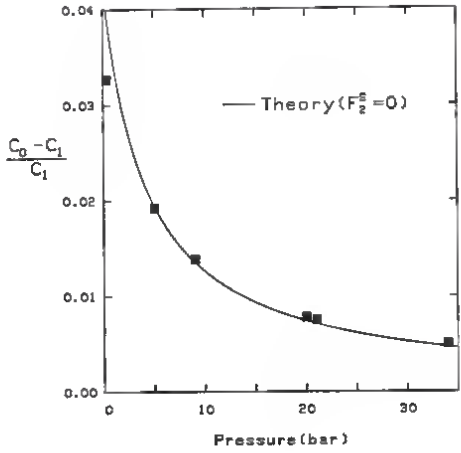

Figure 4–6 Difference of first– and zero–sound velocities vs. pressure. Curve is theory with F_2^s=0

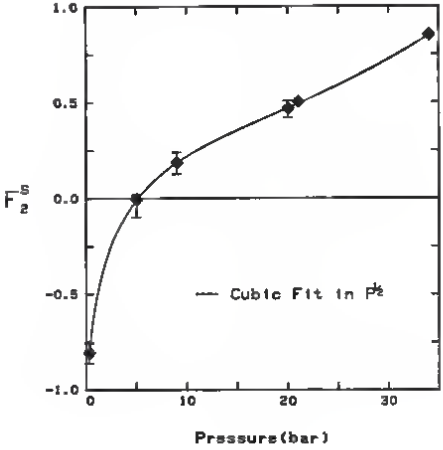

Figure 4-7. F_2^S vs. pressure using F_0^S from Greywall and Busch (1982)

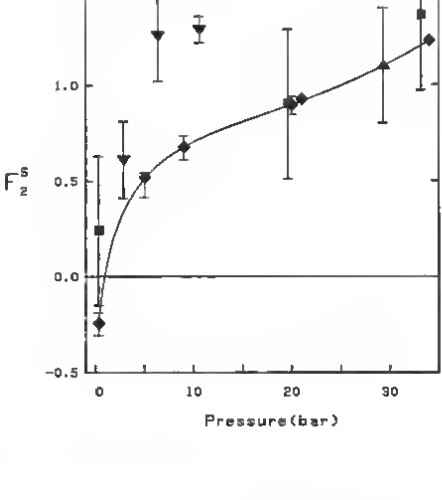

Figure 4–8 F_2^S vs pressure as determined by various workers with F_0^S from Wheatley (1975) This work, diamonds, Abel et al (1966), squares, Ketterson et al. (1975), triangles, Nara et al (1981), inverted triangles

(Abel et al., 1966, Paulson et al., 1973, Ketterson et al., 1975). However, more recent values (Nara et al., 1981) obtained from absolute attenuation measurements are not consistent with these results.

For certain values (Milliken et al., 1981) of Landau parameters, a transverse zero-sound (TZS) mode is predicted to exist

$$F_1^s + 3F_2^s/(1 + \tfrac{1}{5}F_2^s) > 0 \qquad (4.7)$$

Various attempts (Roach and Ketterson, 1976, Flowers et al., 1979) to detect this mode by acoustic impedance techniques have resulted in determinations of F_2^s which are mostly negative, except at very low pressure. Figure 4-9 is a plot of F_2^s as deduced from transverse impedance measurements vs pressure along with the values obtained from this experiment. The values from this work, with the above expression, would preclude the existence of TZS at pressures below 3.4 bars (using scaled values of F_1^s (Greywall and Busch, 1982)). Another feature of the TZS determinations of F_2^s is that they appear to be frequency dependent. The above circumstances lead to the conclusion (Flowers et al., 1979) that these acoustic impedance measurements cannot be analyzed as pure TZS, casting doubt on their determinations of F_2^s.

Conclusions

The fact that sound velocity approaches c_1 as T→0 indicates that there is no change in the density or compressibility due to the formation of the superfluid and that the theoretically expected density mode exists. The precise values of F_2^s determined here, though still very dependent upon determinations of other Landau parameters, can be used to better calculate the responses and properties of normal and superfluid ^{3}He. Because the method used for their deduction did not require

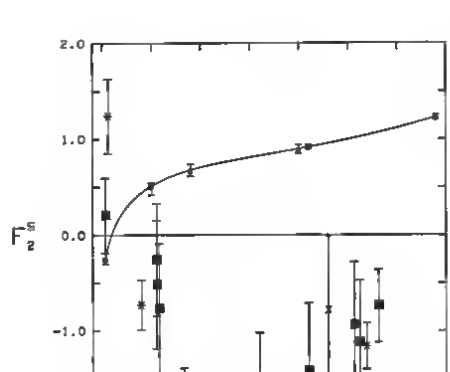

Figure 4–9 Transverse sound determinations of F_2^S. ● This work, ■ Lea et al (1977), ✱ Milliken et al (1979), × Roach and Ketterson (1976)

any absolute measurements of velocity or temperature determinations, these values may easily be adjusted, in the future, as more precise measurements of the other Landau parameters are obtained

CHAPTER 5

NMR MEASUREMENTS OF ^{3}He IN VYCOR

Introduction

This chapter presents nuclear magnetic resonance measurements performed on liquid ^{3}He confined in the pores of Vycor glass and cooled to very low temperatures. Vycor (Corning Glass) is manufactured as a two component glass for ease of handling. Prior to final firing, one of the components is acid leached out leaving multiply connected voids on the order of 20–60 Å. It is the glass at this stage that is used in this experiment as a container for the ^{3}He. Data was systematically acquired as a function of temperature, pressure and magnetic field. The magnetic susceptibility, χ, and transverse dephasing time, τ_2^*, were determined from computer least–squares fits to the digitized free induction decay (FID). Using a simple model to account for the frequency dependence of τ_2^*, the actual spin–spin relaxation time, τ_2, is deduced. In addition, the spin–lattice relaxation time, τ_1, was obtained as a function of temperature at 5 bar.

NMR Measurements

To overcome bandwidth limitations of the digital transient recorder, the free induction decay (FID) response of the confined ^{3}He spins in Vycor was linearly detected (see chapter 3). The resulting envelope was digitized after a small ($\lesssim 10^\circ$) tipping pulse at the Larmor frequency. The captured data were then transferred to the computer for online analysis and recording. Using a variation of the generalized least–squares curve fitting routine *CURFIT* (Bevington, 1969), a single decaying

exponential

$$S(t) = A\,e^{-t/T_2^*} \tag{5.1}$$

was fit to the FID envelope with t=0 defined as the end of the transmitter pulse. Due to amplifier saturation from the incompletely canceled transmitter pulse, the first ≈100 μs interval of the FID was lost in the recovery time of the electronics (see figure 5–1). Hence, to obtain the proper susceptibility, χ, the computer fit was extrapolated to its t=0 value. With typical decay constants on the order of 800 μs, there was plenty of usable signal on which to perform these fits. The decays were indeed fit very well with a single exponential as can be seen in Figure 5–1. In this way, any affect on χ due to variations of T_2^* with temperature or magnetic field is avoided. The inability to have captured signal at the very early received times meant the loss of any quickly decaying resonance signals from the tightly bound ^{3}He spins directly at the surfaces. In an effort to find any missing signal, continuous wave NMR was performed and the lineshape analysed. Figure 5–2 is a typical sweep with a Lorentzian lineshape fit to it. If there were any significant signal with a very broad line, it would have appeared as a contribution in the wings of the Lorentzian. The quality of the fit implies that any signal present from tightly bound spins is indeed very broad and, therefore, not easily detected with our spectrometers. This caused no problems for the study of the ferromagnetically enhanced boundary layers with their exchange narrowed linewidth.

The procedure to attain the data was straightforward, thus allowing unattended computer aquisition. The nuclear cooling stage was precooled to ≈ 24 mK in a magnetic field of 8.5 Tesla. A demagnetization to 96 mT was performed over a period of 12 hours to attain the lowest possible temperature, but leave

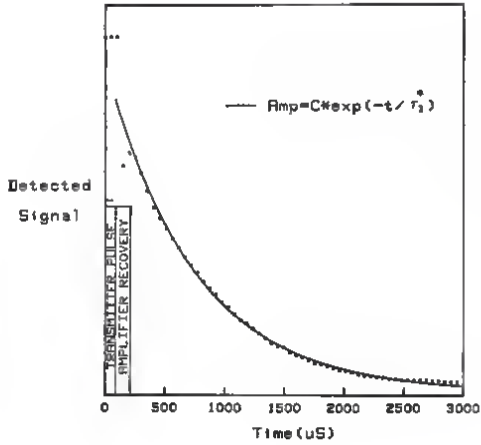

Figure 5–1: Digitized free induction decay envelope and least squares fit

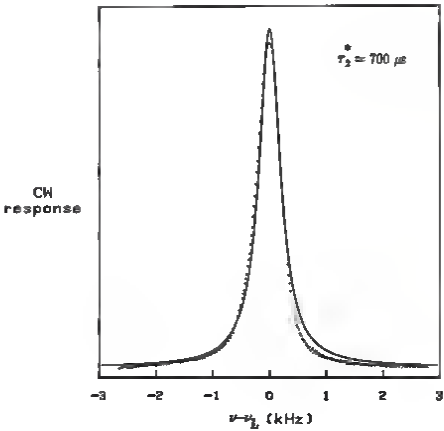

Figure 5–2. Digitized CW–NMR line with Lorentzian fit

enough heat capacity in the Cu bundle to allow a slow warmup Under these conditions, the ^{3}He could be cooled to ~0 3 mK and would warm under the residual heat leak at a rate of ~ 20 μK/h. The Pt thermometer was pulsed every 15 minutes, 1 minute prior to the ^{3}He NMR pulse When the system approached the transition temperature of the bulk superfluid, T_{c1}, the ultrasound cell was activated in order to obtain a fixed point calibration for the Pt thermometer As the bulk fluid went through the transition, an easily distinguishable drop in the sound amplitude was observed

The thermal time constant of the ^{3}He in the Vycor was determined to be ~1h by watching the recovery of the susceptibility after administering a large heat pulse Figure 5–3 shows the response of the NMR signal, measured with small angle tipping pulses, as a function of time after a 90° pulse at ~ 0.5 mK It is not clear where the source of this rf heating is actually coming from in response to the large pulse, however, the ^{3}He spins respond very quickly indicating that the Vycor itself is warming. A single exponential with a time constant of one hour fits the data well Thus, at the above stated warming rate, the various probes (Pt thermometer, ultrasound cell) are all in good thermal equilibrium with the NMR cell

Magnetic Susceptibility

The susceptibility as a function of temperature below 10 mK is shown for six pressures in figures 5–4a–f. Because χ was inversely proportional to temperature, the amplitude of the NMR response would change by a factor of ~100 over the temperature range 0 3 mK $\leq T \leq$ 30 mK To keep the signal within the linear operating range of the amplifier chain, step increases in the transmitter power (and hence tipping angle) were periodically performed as the sample warmed Constant temperature tests of NMR response versus power indicated no unusual tipping angle dependence. In the analysis of the susceptibility versus temperature, discontinuities

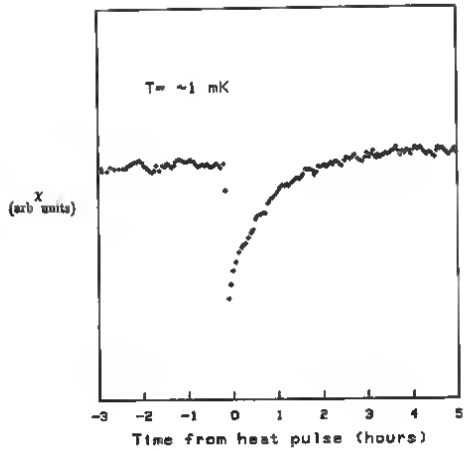

Figure 5-3 Susceptibility recovery from a heat pulse.

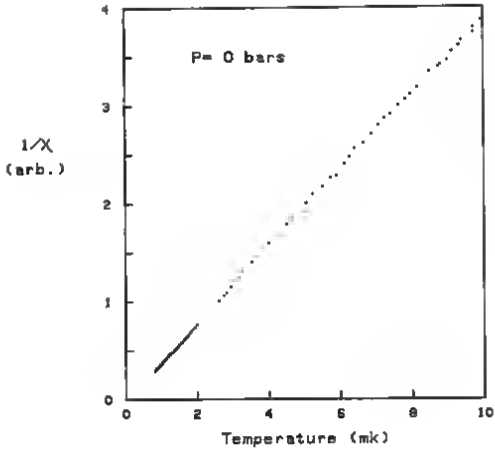

Figure 5–4a. Inverse susceptibility vs. temperature at 0 bars

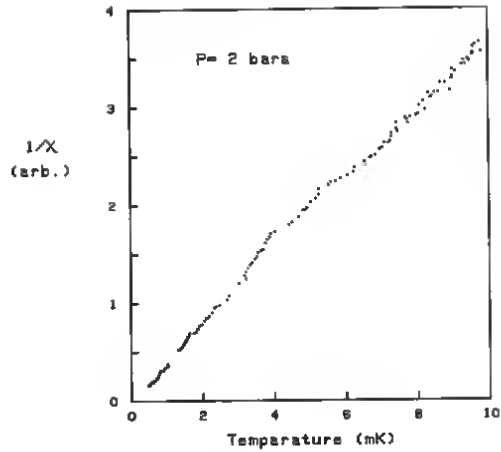

Figure 5–4b Inverse susceptibility vs. temperature at 2 bars

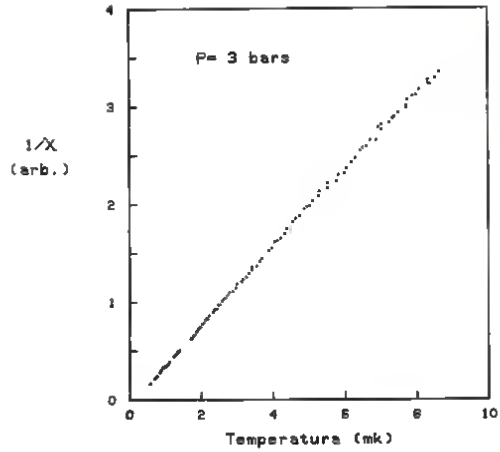

Figure 5–4c Inverse susceptibility vs temperature at 3 bars

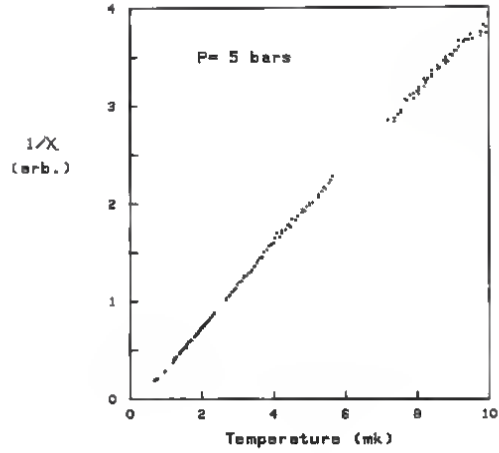

Figure 5-4d Inverse susceptibility vs temperature at 5 bars.

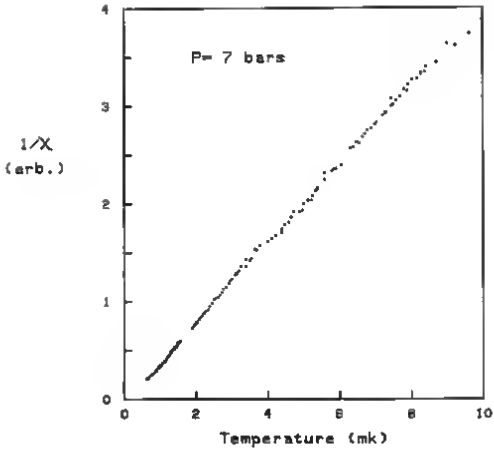

Figure 5–4e. Inverse susceptibility vs temperature at 7 bars.

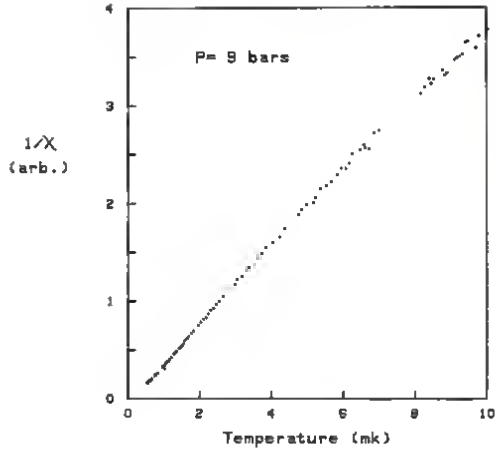

Figure 5–4f. Inverse susceptibility vs temperature at 9 bars

due to power changes were accounted for by scaling with the ratio of the magnitudes just before and after the change. Because of the very slow warming rate, these different power points were at essentially the same temperature and thus the final scaled data fell on a very smooth curve. Any tipping angle dependence would have appeared as a discontinuous change of slope in these data.

The resulting χ vs T data were fit very well by

$$\chi = \frac{C}{T-\theta} + \chi_p \qquad (5.2)$$

which is a Curie–Weiss law with the addition of a temperature independent term, χ_p, indicative of a degenerate Fermi liquid (see figure 5–6). As the pressure of the bulk liquid ^{3}He feeding the Vycor rod from both ends is changed, the values of the Curie constant, C, the Weiss temperature, θ, and χ_p also change. However, because the NMR response is dependent on several uncontrollable factors, i.e. $\vec{H}_0$ homogeneity, $\vec{H}_1$ homogeneity, amplifier gain, etc. the magnitude of χ cannot be determined absolutely. This fact only affects the determination of C and χ_p because θ depends only on the temperature scale. In many other confined geometry experiments (see chapter 2), the pore size and geometry are such as to allow a large amount of bulk liquid to be present. In many respects this presents a problem when trying to decipher contributions from walls, confining pores, bulk liquid and the presence of superfluid. However, in one respect it can be used to an advantage. If the NMR signal from the ferromagnetically enhanced surface ^{3}He is a small contribution compared to the bulk, then at a high enough temperature (~100 mK) the sample will behave entirely bulk–like and χ will be temperature independent. This then is an in–situ standard for calibration of the magnitude of χ. Thus, when the pressure is changed, C and χ_p can be compared by relating to the bulk value.

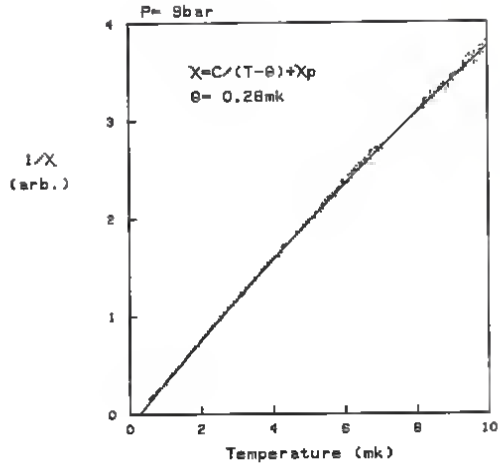

Figure 5–5 Typical Curie–Weiss fit to χ^{-1} vs. T.

in the Vycor cell used in this experiment, the above procedure will not work The susceptibility is found to vary as $\sim 1/T$ from the lowest temperatures continuously to 2 K (see fig 5–6) There is no bulk liquid behavior, which in one sense is good since we can probe the truly confined ^{3}He, but we therefore cannot compare χ to anything in–situ Thus, to compare the Curie constant as a function of pressure, we must rely on the electronics having stable behavior from one pressure to the next, which for the range covered took several months Unfortunately, this proved to be impossible

One parameter that can be determined with high precision is the Weiss temperature, θ On a plot of $\frac{1}{\chi}$ vs T, θ is the T intercept (see figure 5–5). It, therefore is independent of the absolute magnitude of χ and is affected only by the accuracy of temperature determination Because expression (5.2) fits the data so well over the entire temperature range and because the sample was cooled so closely to the extrapolated transition temperature, the uncertainty of θ was ≤ 10 % Figure 5–7 shows the Weiss θ versus pressure The θ is always positive indicating a ferromagnetic tendency and varies from 0 13 mK at 0 bar to 0 28 mK at 9 bar Unfortunately the data stops at 9 bar due to weaknesses in the epoxy cell body

Spin–Lattice Relaxation

The spin–lattice relaxation time, τ_1, was measured at a pressure of 1 1 bar and a magnetic field of 289 Gauss The data as a function of temperature appear in figure 5–8 The monotonically increasing, nearly linear behavior is similar to other measurements of restricted ^{3}He (Kelley and Richardson, 1974, Godfrin et al , 1978) In the interest of looking for magnetic coupling to spins within the substrate as seen in the experiments on fluorocarbon microspheres (Friedman et al , 1981), the magnetic field was adjusted to the Larmor resonance for Si (Vycor is predominantly SiO_2) Figure 5–9 shows the time recovery of the silicon signal after saturation at

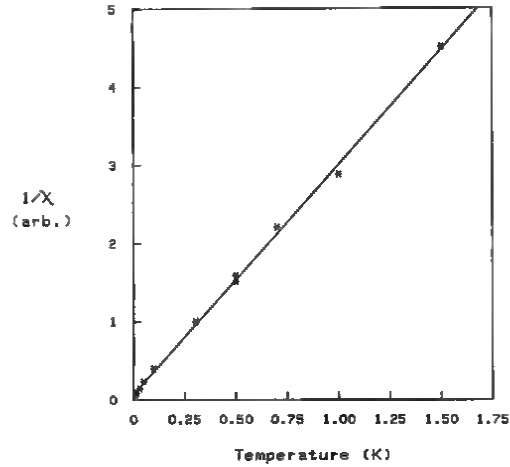

Figure 5–6 Inverse susceptibility vs T to log$_4$ temperature.

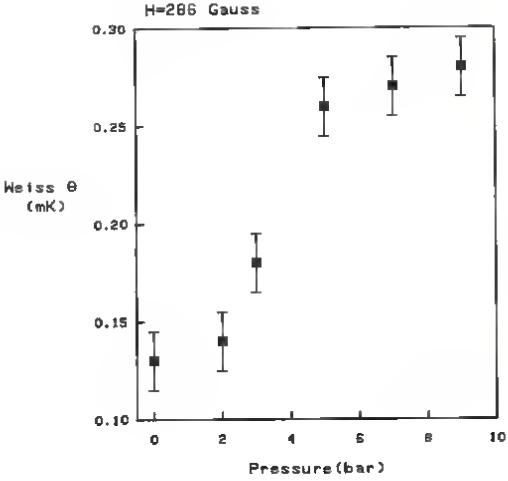

Figure 5–7 Weiss temperature, θ, vs pressure.

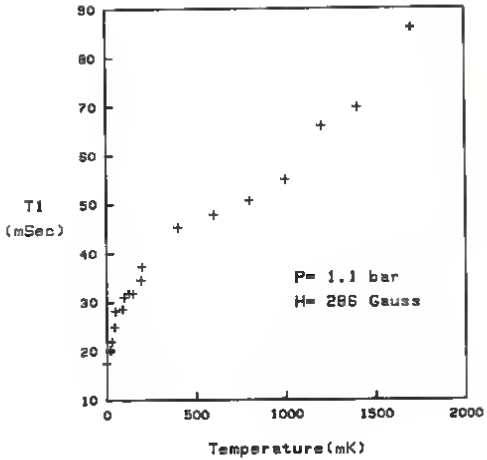

Figure 5–8. Spin–lattice relaxation time τ_1, vs. temperature.

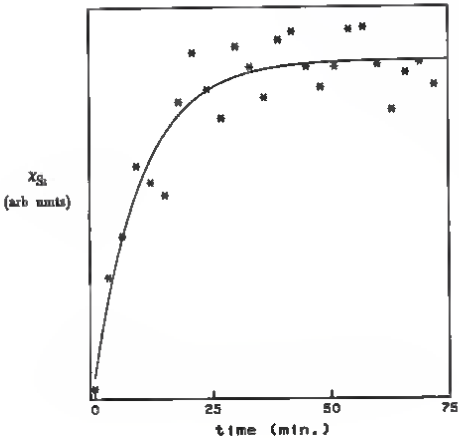

Figure 5–9 Susceptibility of Si vs time used to determine the spin lattice relaxation time, τ_1, of Si spins in the Vycor glass

20 mK An exponential fit gives a τ_1 on the order of 10 minutes. This would appear to be very fast for the relaxation of a glass at these low temperatures, however, it is still very long compared to τ_1 of the ^{3}He, which is on the order of tens of milliseconds. Thus, the large surface area does reduce the relaxation time of the Si spins, but no evidence for direct magnetic coupling was seen.

Measured Spin Dephasing Time, τ_2^*.

The time constant of the free induction decay, τ_2^*, is a measure of the dephasing time of the spins after being coherently excited with the transmitter pulse. This measured time, however, is affected by both the inherent microscopic dynamics of the system as governed by the spin–spin relaxation time, τ_2, as well as magnetic field inhomogeneities which cause different parts of the sample to precess at different frequencies. In order to obtain a meaningful and apparatus independent measure of the intrinsic τ_2, this field inhomogeneity effect must be accounted for. The traditional approach in pulsed NMR is to use a variation of a 90°–180° pulse sequence to obtain a spin echo which removes the effect of the external field inhomogeneity by rephasing the spins that were dephased by the field gradient. Unfortunately, as pointed out previously, at the very low temperatures of this experiment, the rf heating due to large pulses causes severe problems. Thus, an alternative method had to be devised.

Deduction of Spin–Spin Relaxation Time, τ_2.

In a homogeneous medium in an inhomogeneous magnetic field, the measured dephasing time can be written as

$$\frac{1}{\tau_2^*} = \frac{1}{\tau_2} + \gamma \Delta H \qquad (5.3)$$

where τ_2 is the actual spin–spin relaxation time, γ is the gyromagnetic ratio, and ΔH is the field deviation over the sample. This expression can be rewritten in terms of frequency as

$$\frac{1}{\tau_2^*} = \frac{1}{\tau_2} + \omega\left[\frac{\Delta H}{H}\right] \tag{5.4}$$

where $\Delta H/H$ is now the fractional deviation of the field. From this relation it is possible to extract τ_2 directly from the frequency dependence of τ_2^* if this linear behavior of the inverse holds. Figure 5–10 displays τ_2^* versus temperature at five different frequencies at a pressure of 5 bar. There is obviously a strong temperature dependence which itself depends on the measuring frequency for the sign of the behavior. From the raw data it is not obvious that equation (5.4) is applicable, however, constant temperature slices on figure 5–10 were taken and $\left[\tau_2^*\right]^{-1}$ vs ω plotted in figure 5–11. The surprising result is that this quantity has a linear behavior at all temperatures as in equation (5.4), but with temperature dependent slopes and intercepts. Ordinarily, the $\frac{\Delta H}{H}$ term is determined by the quality of the external magnet and is therefore temperature independent. The fact that it is temperature dependent in these data implies that the ^{3}He is somehow affecting the field homogeneity at low temperature.

To understand this dependence, $\frac{\Delta H}{H}$ vs T is plotted in figure 5–12. A least–squares fit of the form

$$\frac{\Delta H}{H} = \frac{a}{T-\theta} + \left[\frac{\Delta H}{H}\right]_{ext} \tag{5.5}$$

is shown as the solid curve and fits very well. The first term has the same temperature dependence as the ^{3}He susceptibility where, to within the precision of

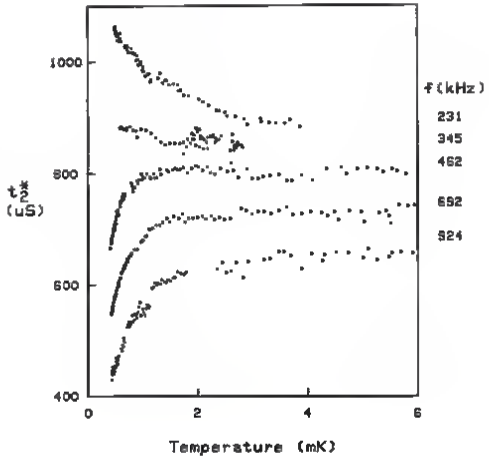

Figure 5–10 Spin dephasing time, τ_2^*, vs T for five frequencies

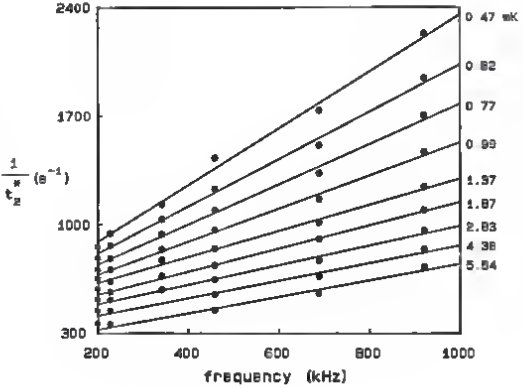

Figure 5–11 Inverse of T_2^* vs frequency displaying linear behavior

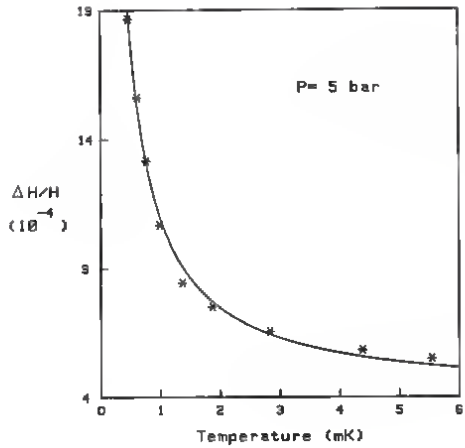

Figure 5–12 Effective field inhomogeneity vs temperature

these data, θ is the same Weiss temperature as found for χ. Hence, the highly polarized ^{3}He spins are disturbing the overall effective field homogeneity. This is easily understood when considered in the light of frequency shift measurements of ^{3}He in Grafoil (Bozler et al., 1983). As described in chapter 2, Grafoil is an exfoliated graphite which has very well defined parallel planes. The ^{3}He in the surface magnetic state then sees a fixed relationship between the surface normal and the direction of the external field. When the spins become highly polarized, the local magnetic field that a ^{3}He spin experiences is changed and the Larmor frequency is shifted. The magnitude of this shift depends on the relative orientation of the surface and the external field as seen in figure 2-6 from the work of Bozler et al., 1983. Now in Vycor, there is no fixed relationship of the surface normal and the field. The randomly oriented pore walls then give a spread in frequencies, or effectively a line broadening, and thus the measured field homogeneity degrades as the spins become more highly polarized. As a consistency check of this interpretation, the extrapolated high temperature value of $\frac{\Delta H}{H}$ should be that for the external magnet without any effect of the ^{3}He. Indeed, $\left[\frac{\Delta H}{H}\right]_{T=\infty} = \left[\frac{\Delta H}{H}\right]_{ext} = 4 \times 10^{-4}$ as previously determined by line width measurements of bulk liquid ^{3}He in this magnet.

With the above consistent analysis, the interpretation of the y-intercept term as $(\tau_2)^{-1}$ is certainly valid. The apparatus dependent and polarization effects have therefore been accounted for and the true spin-spin relaxation behavior obtained. Figure 5-13 shows τ_2 vs T with the solid curve being a least-squares fit of

$$\tau_2 = \frac{b}{T-\theta} + \left[\tau_2\right]_{\substack{\text{exchange} \\ \text{narrowed}}} \qquad (5\,5)$$

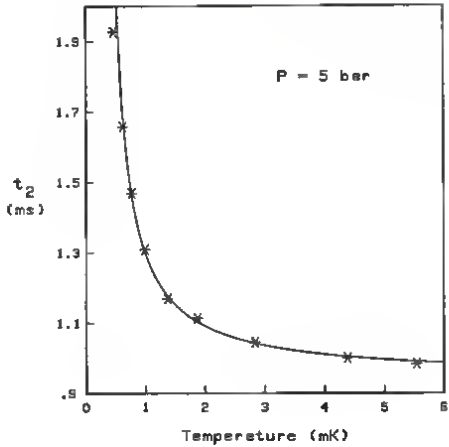

Figure 5–13 Deduced true spin–spin relaxation time, τ_2, vs temperature

Again, to within the experimental uncertainties, this θ is the Weiss temperature as measured with susceptibility, but the precision of this determination is nowhere near that as from χ. So the intrinsic τ_2 increases as the temperature is lowered leading to a narrowing of the NMR line. It is now clear where the puzzling frequency--temperature dependence of τ_2^* is coming from. The polarisation is degrading the field homogeneity and causing the line to broaden (τ_2^* decreases). This effect is weighted by the NMR frequency since τ_2^* is the dephasing *time* of the precessing spins, i.e. at a given temperature the spins get out of phase in the same number of cycles regardless of the frequency, but the time to dephase decreases as the frequency is increased. At the same time, the intrinsic linewidth is decreasing (τ_2 increases) leading to a competition of terms in equation (5.4). Figure 5-14 shows how the fits of $(\tau_2)^{-1}$ vs. T and $\frac{\Delta H}{H}$ vs. T can be recombined using equation (5.4) to produce the solid curves. The fits have no additional adjustable parameters and account for the behavior well. It is interesting to note the almost total lack of temperature dependence of the 345 kHz data. This fortuitous cancellation at this frequency is uniquely determined by the overall homogeneity of the NMR magnet and totally masks the strong temperature dependence of τ_2.

Magnetism and Flow Interactions

Another interesting effect is the behavior of the enhanced magnetism when the ^{3}He is made to flow through the Vycor. Early evidence of this interaction was observed in the experiment of Spencer (1986), though no firm conclusions could be drawn due to the inseparability of heating effects. Figure 5-15 displays the susceptibility as a function of time when a pressure head is impressed across the Vycor rod. The differential pressure was monitored with a Kapton diaphragm manometer capacitively measured with a ratio transformer bridge. The ^{3}He pump was stroked to a fixed position and the liquid allowed to relax the pressure through

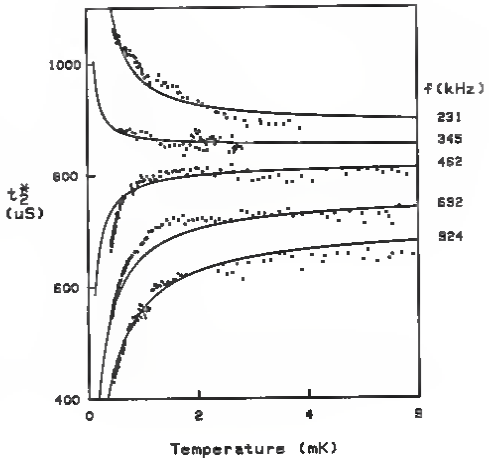

Figure 5–14 Spin dephasing time, T_2^*, vs T at five frequencies Curves are reconstructed behavior from model described in text

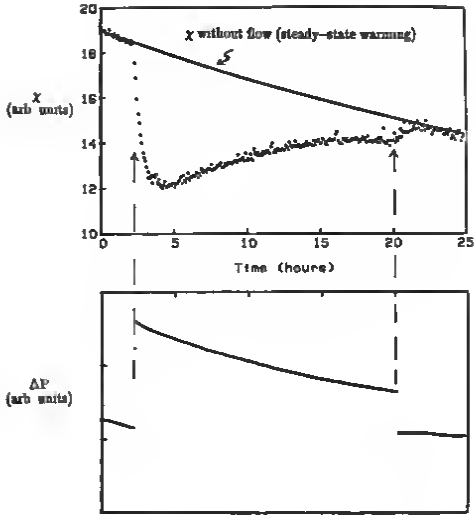

Figure 5–15 Susceptibility response to flow

the Vycor The susceptibility is suppressed as the ^{3}He flows by an amount dependent on the pressure head, however, this is consistent with a rise in temperature in the Vycor due to viscous heating. In fact, when the flow is halted, the susceptibility recovers with the characteristic thermal time constant previously discussed

To remove thermal effects and, thereby, reveal any fundamental relation between flow and magnetism, the dephasing time τ_2^* was monitored simultaneously with the susceptibility If there was no intrinsic change in the magnetic state due to flow, then both χ and τ_2^* would change by amounts consistent with a temperature increase Using the fit temperature dependences from the non–flowing data, one parameter can be used as an in–situ "thermometer" to remove changes due to heating in the other In figure 5–16, an Arrhenius law fit to the nonflowing τ_2^* is shown Thus fairly good fit, therefore, allows τ_2^* to he used as a measure of the temperature of the ^{3}He actually in the Vycor If this temperature is now used with the previously determined Curie–Weiss law for the system at this pressure, the susceptibility, χ_0, due to just thermal effects can be predicted.

Figure 5–17 shows the raw susceptibility, χ (light points), and the normalized difference, $\frac{\Delta\chi}{\chi} = (\chi - \chi_0)/\chi_0$ (dark points), plotted versus time during a 50 hour period during which there were large overall temperature changes and high flow rates In the figure, there was cooling without flow (to A), increasing flow (to B), decreasing flow (to C), more cooling because the flow was halted (to D) and then warming without flow As is evident in the regions without flow (all but A to C), the difference, $\frac{\Delta\chi}{\chi}$, is zero and unchanging even the though the overall temperature is changing by large amounts This proves that temperature changes due to viscous heating effects in the flowing liquid can he successfully removed to leave only those changes due to an altering of the magnetic state by flow If there were no direct effect of the flow on the ^{3}He magnetism, then $\frac{\Delta\chi}{\chi}$ should remain zero

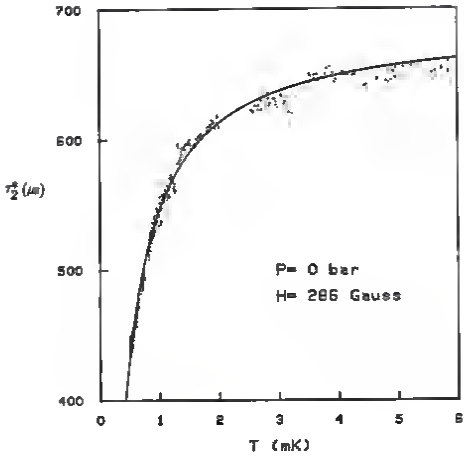

Figure 5–16 Fit of τ_2^* vs T for use as in-situ thermoter during flow

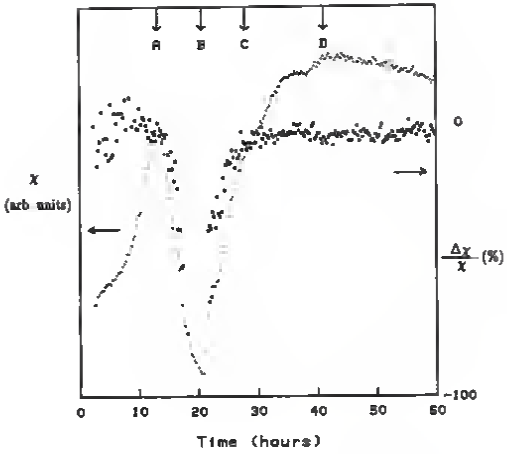

Figure 5–17 Flow behavior with heating effects removed (see text for description.)

regardless of the conditions imposed. Obviously, from A to C, this not the case. There is as much as a 50% reduction of the susceptibility by flowing the liquid.

In actuality, the above analysis, while definitely showing a flow effect on the magnetism, cannot determine whether it is χ or τ_2^* that is affected or both. It is only a measure of the relationship between these two parameters. One simple interpretation is that the spin relaxation processes are on a timescale that is short compared to that of the flow and, hence, τ_2^* is not directly affected. Then, the reduction of the susceptibility can arise from the removal, by the flow, of spins from the localized surface state and into the low susceptibility degenerate liquid.

Conclusions

The magnetic susceptibility measurements presented are consistent with ^{3}He on other substrates (see chapter 2 for a description of other work). The pressure dependence of the Weiss θ, when viewed in the context of exchange mechanisms, may indicate a modification of the exchange frequencies by the increase in density. The very sensitive dependence should, therefore, be addressed by theory. In addition, these are the first low temperature measurements of the actual spin–spin relaxation time, τ_2. The Curie–Weiss like temperature dependence of τ_2, with its line narrowing as the temperature is decreased, should be predictable from theory. It is possible that it is an indication of the dimensionality of the phase transition (Richards, 1976). The temperature independent value of $\tau_2 \approx 900$ μs above 10 mK is narrowed above that of bulk solid, and should, therefore, be an indirect measure of the pertinent exchange frequency.

Chepter 6

CONCLUSIONS AND FUTURE WORK

The experiments presented in this dissertation explore the nature of order in quantum systems at very low temperatures Helium–3 has become the system of choice for these kind of studies not only because of its rich behavior, but also because of its high purity and availability Unlike many solid state phenomena, the behavior of ^{3}He at low temperatures is sample independent and uncomplicated by the presence of impurities The theory can, therefore, attempt to account for the phenomena that are fundamental to this system

Ultrasound in Liquid ^{3}He

The ultrasound experiment on normal and superfluid ^{3}He resolved the origin of a curious apparatus dependent effect, confirmed a long standing theoretical prediction, and provided improved values of the Landau parameter F_2^s. The values of F_2^s presented, while consistent with earlier determinations, are of a high enough precision to allow a more detailed comparison of theory and experiment Many theoretical predictions, such as the existence and location of order parameter collective modes in superfluid ^{3}He, depend upon many experimentally determined parameters A precise and consistent set of Landau parameters is, therefore, essential for a meaningful test of the theory

One drawback of the ultrasound experiment was its relatively low frequency of 5 MHz. Unfortunately, due to apparatus limitations, this could not be raised As a result, the determination of the zero–sound velocity had to be corrected for finite

$\omega\tau$. Though this was not difficult, it does add an unnecessary step and, hence, uncertainties. As a check, the velocity should be measured at higher frequencies. (Note: the next experiment being built in this laboratory will have this capability.)

Magnetism of ^{3}He in Vycor

The NMR experiment on liquid ^{3}He confined in Vycor glass displayed many interesting and unexpected phenomena. The strong pressure dependence of the Weiss θ is suggestive of a change in the exchange environment that the surface spins are in. To correlate this behavior with the number of solid-like atoms near the surface, a future experiment should be able to measure the Curie constant (proportional to the number of spins) absolutely or at least relative to a known reference. In this way, if the number of atoms participating in the ferromagnetic exchange changes with pressure, it can be detected.

Though complicated and not well characterized, the random pore structure of Vycor was used to an advantage for the deduction of τ_2. The changeover behavior seen in τ_2^* as a function of frequency emphasizes the need to determine the actual τ_2 before any conclusions can be drawn. For future experiments, a more straight-forward method for determining τ_2 should be developed for ultra-low temperatures (e.g. small angle spin echoes). Correlations between the pressure dependences of θ and τ_2 can then be studied in order to form a more unified picture of particle exchange in these systems.

The flow and magnetism interactions displayed in this experiment emphasize the subtle nature of the surface magnetic state. Coupled with the interesting and very complicated flow measurements performed by G.F. Spencer for his Ph.D. dissertation (1986), a consistent picture of the behavior of liquid ^{3}He in very confined geometries can be pursued. Future work could entail flow studies in more regular geometries (possibly produced by micro-electronics photo-lithographic

techniques)

One final and intriguing possibility is the use of confined geometries to form highly polarized normal liquid ^{3}He. If the polarization of the surface state is maintained into the nearby liquid and can be clearly separated in the analysis, many predictions for a highly polarized Fermi liquid may be tested

REFERENCES

W R. Abel, A C Anderson and J C Wheatley (1962) Phys Rev Lett 17, 74.

A.I Ahonen, T A Alvesalo, T Haavasoja, and M C Veuro (1978) Phys Rev Lett 41, 494

A.I Ahonen, T Kodama, M Krusius, M A Paalanen, R.C Richardson, W Schoepe, and Y Takano (1976) J Phys C 9, 1655

P W Anderson (1958) Phys Rev 112, 1900

P W Anderson and W F Brinkman (1978) in The Physics of Liquid and Solid Helium, Part 2, K B Bennemen and J B Ketterson, eds , Wiley & Sons, New York

J L Bardeen, N Cooper, and J R. Schrieffer (1957) Phys Rev 108, 1175

M T Beal–Monod and S Domach (1977) J Low Temp Phys 28,175

R.F Berg (1983) Ph.D Dissertation, University of Florida.

R.F Berg and C G Ihas (1984) Rev Sci Instrum 55, 1174

P R Bevington (1969) Data Reduction and Error Analysis for the Physical Sciences, McCraw–Hill, New York

N N Bogoliubov, V V Tolmachev, and D N Shirkov (1959) in New Method in the Theory of Superconductivity, Consultants Bureau, New York

H M Bosler, T Bartolac, K Luey, and A L Thompson (1978) Phys Rev Lett 41, 490

H M Bosler, D M Bates, and A L Thompson (1983) Phys Rev B 27, 6992

D F Brewer (1970), J Low Temp Phys 3, 205

D F Brewer and J S Rolt (1972) Phys Rev Lett 29, 1495

B P Cowan, M G Richards, A L Thompson, and W.J Mullin (1977) Phys Rev Lett 38, 165

J M Delrieu, M Roger, and J H Hetherington (1980) J Low Temp Phys 40, 71

B N Engel, R.F Berg, and G G Ihas (1985) Phys Rev Lett 54, 1331

B N Engel and G G Ihas (1985) Phys Rev Lett 55, 955

E G. Flowers, R.W Richardson, and S.J Williamson (1976) Phys Rev Lett 37, 309

H Franco, R.E. Rapp and H Godfrin (1986) Phys Rev Lett 57, 1161

L J Friedman, P Millet, and R.C Richardson (1981) Phys Rev Lett 47, 1078

L.J Friedman, S N Ytterboe, H M. Bosler,, A L Thompson, and M C Cross (1988) Phys Rev Lett 37, 2843

E Fukushima and S Roeder (1981) Experimental Pulse NMR: A Nuts and Bolts Approach, Addison–Wesley, Reading, Massachusetts.

R.W Cianetta (1980) Ph.D Dissertation, Cornell University

H. Godfrin, G Frossati, D Thoulouse, M Chapellier, and W G Clark (1978) J Phys (Paris), Colloq 39, C6–287

D S Greywall (1986) Phys Rev B 33, 7520

D S Greywall and P A Busch (1982) Phys Rev Lett 49, 146

G G Ihas, B.N Engel, and R.F Berg (1985) Phys Lett 109A, 105

H Jichu and Y Kuroda (1982) Prog Theor Phys 67, 715

T Kanaya (1956) Prog Theor Phys 16, 48

J Kelly and R.C Richardson (1974) in Low Temperature Physics, LT 13, W J O'Sullivan, K D Timmerhaus and E F Hammel, eds , Plenum Publishing, New York

J B Ketterson, P R. Roach, B M Abraham, and P D Roach (1975) in Quantum Statistics and the Many–Body Problem, S B Trickey, W P Kirk, and J W Dufty, eds , Plenum Publishing, New York

L D Landau (1959) Zh Eksp Teor Fiz 30, 1058 (English translation JETP 3, 920)

L D Landau (1957) Zh Eksp Teor Fiz 32, 59 (English translation JETP 5, 101)

M J Lea, K J. Butcher, and E R. Dobbs (1977) Commun Phys 2, 59

A.J Leggett (1975) Rev Mod Phys. 47,331

M W Meisel (1983) Ph D Dissertation, Northwestern University

F P Milliken, R.W Richardson, and S J Williamson (1976) Phys Rev Lett 36, 739

K A Muething (1979) Phd Dissertation, Ohio State University

K Nara, I Fujii, K. Kaneko, and A Ikushima (1981) Physica (Amsterdam) 108B+C, 1203

Y Okuda, A J Ikushima, and H Kojima (1985) Phys Rev Lett 54, 130

D D Osheroff, R.C. Richardson, and D.M Lee (1972) Phys Rev Lett 28, 885

D N Paulson, R J Johnson, and J C Wheatley (1973) Phys Rev Lett 30, 829

D N Paulson and J C Wheatley (1978) Phys Rev Lett 41, 254

P M Richards (1978) in Local Properties at Phase Transitions, K A Mueller and A. Rigamonti, eds , Proceedings of the Enrico Fermi International Summer School of Physics, Varenna, 1978, Vol 59, North–Holland, New York

R.C Richardson and D M Lee (1978) in The Physics of Liquid and Solid Helium, Part 2, K H Benneman and J B Ketterson, eds , Wiley & Sons, New York

P R. Roach and J B Ketterson (1976) Phys Rev Lett 36, 736

M Roger and J M Delrieu (1987) Jap Journ Appl Phys 26–3, 267

M A Ruderman and C Kittel (1954) Phys Rev 96,99

D Spanjaard, D L Mills, and M T Beal–Monod (1979) J Low Temp Phys. 34, 307

G F Spencer (1986) Ph.D dissertation, University of Florida.

G C Straty and E D Adams (1969) Rev Sci Instrum 40, 1383

J C Wheatley (1975) Rev Mod Phys 47,415

P Wölfle (1973) Phys Rev Lett 31, 1437

P Wölfle (1978) in Progress in Low Temperature Physics, Vol. 7A, D F Brewer, ed North–Holland, New York

K. Yosida (1957) Phys Rev 106, 893

BIOGRAPHICAL SKETCH

Bradley N Engel was born on March 20, 1959, in Miami, Florida. Growing up in the space age, his thoughts and interests were dominated by science and technology. In his early teens, he became interested in astronomy and pursued this hobby with vigor. After attending high school at Miami Palmetto Senior High, he entered the University of Florida. The first two years there were uninspiring and Brad's interest in science began to wane. Deciding that the formal class structure needed a supplement, he began looking for a professor that would provide an independent research project. It was his good fortune that he connected with Professor Gary Ihas and was given a chance to experience the wonders of low-temperature experimental physics. The compatibility he felt with this area of physics is something rare.

After completing his bachelor's degree, Brad attended graduate school in physics at the University of Michigan where he was given a research assistantship due to his experimental background. Fortunately, the type of research he became involved in did not provide the same enjoyment as did low-temperature physics, and so he returned from whence he came to obtain his Ph.D. with Professor Ihas.

I certify that I have read this study and that in my opinion it conforms to acceptable standards of scholarly presentation and is fully adequate, in scope and quality, as a dissertation for the degree of Doctor of Philosophy

Gary G Ihas Chairman
Professor of Physics

I certify that I have read this study and that in my opinion it conforms to acceptable standards of scholarly presentation and is fully adequate, in scope and quality, as a dissertation for the degree of Doctor of Philosophy

E Dwight Adams, Cochairman
Professor of Physics

I certify that I have read this study and that in my opinion it conforms to acceptable standards of scholarly presentation and is fully adequate, in scope and quality, as a dissertation for the degree of Doctor of Philosophy

Neil S Sullivan
Professor of Physics

I certify that I have read this study and that in my opinion it conforms to acceptable standards of scholarly presentation and is fully adequate, in scope and quality, as a dissertation for the degree of Doctor of Philosophy

Pradeep Kumar
Professor of Physics

I certify that I have read this study and that in my opinion it conforms to acceptable standards of scholarly presentation and is fully adequate, in scope and quality, as a dissertation for the degree of Doctor of Philosophy

Dr. Stephen T. Gottesman
Professor of Astronomy

This dissertation was submitted to the Graduate Faculty of the Department of Physics in the College of Liberal Arts and Sciences and to the Graduate School and was accepted as partial fulfillment of the requirements of the degree of Doctor of Philosophy

August 1988

Dean, Graduate School